Addressing the effects of inaccurate top-salt delineation on subsalt seismic imaging

Guillaume Barnier and Biondo Biondi

ABSTRACT

Imaging in the presence of salt bodies is important for the oil and gas industry but, it is also very difficult. Current seismic imaging techniques may still fail to capture the fine-scale details of a rugose boundary between the top of a salt body and its overlying sediments. This lack of accuracy can have a destructive effect on images of potentially hydrocarbon-bearing layers located underneath the salt. In this paper, we give an overview of the main challenges encountered by the oil and gas industry in terms of subsalt imaging, and we explain the importance of addressing the problem of top-salt boundary delineation. We conduct synthetic tests, and show that a slight misinterpretation of a top-salt boundary significantly damages the image quality of underlying layers. Image gathers may become incoherent and uninterpretable, which prevents us from using standard migration velocity analysis techniques to improve imaging. There is a need to develop a technique that enables us to refocus the subsalt images. We propose an approach for future research.

INTRODUCTION

Oil and gas companies are expanding their search for hydrocarbons into zones with increasing geological complexity, such as sedimentary basins containing allochthonous salt bodies. Unfortunately, seismic imaging around salt is difficult. One of the main challenges is the lack of accuracy in the subsurface velocity model. More specifically, a problem that has recently drawn a great deal of attention is the limitation of currently existing techniques to accurately delineate the interface between the top of a salt body and its overlying sediments, and the impact is has on the image-quality of deeper layers (Halpert, 2014; Etgen et al., 2014a,b; Albertin et al., 2014). Because this interface is usually very rugose and may take complex geometrical shapes, it is difficult to resolve its very fine-scale features. The velocity contrast between the salt body and its surrounding sediments is so high that the quality of the seismic image beneath this interface is highly sensitive to the accuracy of the boundary location. Even a slight error in the interpreted location of this interface can have a disproportionate impact on the calculations of wave propagation beneath the interface, and lead to significant degradation of the resulting image (Halpert, 2014). In the first part of this paper, we explain why salt basins are relevant and attractive in hydrocarbon exploration, we describe where the main challenges lie, and we discuss the importance of getting more

accurate and well-focused subsalt images. In the second part, we analyze into more detail the difficulty in precisely delineating the top-salt boundary, and we explain why present techniques may fail to do so. In the third and fourth part, we present synthetic examples that illustrate the effects of inaccurate top-salt delineation on the image-quality of subsalt layers, and the need for a new algorithm to address this issue. In the last part, we discuss the possible approaches we intend to take to solve this problem.

SALT BASINS IN HYDROCARBON EXPLORATION

Salt basins are attractive zones for oil and gas exploration, and remain among the best places to find hydrocarbon reserves worldwide. The best-known salt basins are located in the Gulf of Mexico, the Persian Gulf, the North Sea, the West African margin, and the Brazilian margin. However salt basins, especially tertiary basins with allochthonous salts, are difficult places to explore because of poor subsurface images obtained around and below salt (Leveille et al., 2011). In this section, we propose a literature review of the main geological and geophysical properties of salt basins, and we summarize the challenges the industry currently faces when imaging in the presence of salt bodies.

Geological properties of salt bodies

Salt is an evaporite, and salt beds are formed by the natural evaporation of the sea water from an enclosed basin. The precipitated salt layer is then buried by successive layers of sediments over geologic time until segments of it begin to flow upward toward the surface of the Earth, thereby creating a salt dome (DNR, 2015). A salt dome is a mound or column of halite that has been pushed upward from below through the surrounding rocks and sediments into its present position. Rock salt (i.e., halite) has two properties that enable it to form salt domes.

- When it is buried to depths greater than a few 100 meters, salt will have a density of approximately 2.16 g/cm^3, which is much lower than most other sedimentary rocks (e.g., shales, limestones, etc.). These sedimentary rocks tend to have lower densities when they are deposited because they contain a lot of water. As the depth of burial increases, the density of salt remains about the same, but the mass density of shales and limestones increases as the water is squeezed from their pore space. Eventually, their mass density might reach values ranging from 2.4 g/cm^3 to 2.7 g/cm^3, which is much higher than the salt's mass density (King, 2015).
- Salt also has the ability to deform and flow like a high-viscosity fluid when it is under pressure.

The overlying sediments tend to exert a compressive, downward force; and if the rock sequence is also subjected to tectonic forces, salt may begin to flow upward like a plastic substance. A small fracture in the overlying, higher-density sediments can trigger the upward movement. While compression forces will produce folding, and salt domes might erupt through the crest of anticlines (Figure 1); extension forces will produce thinning and normal faulting, which might create weaknesses that the salt might exploit (Figure 2)(Hudec and Jackson, 2007).

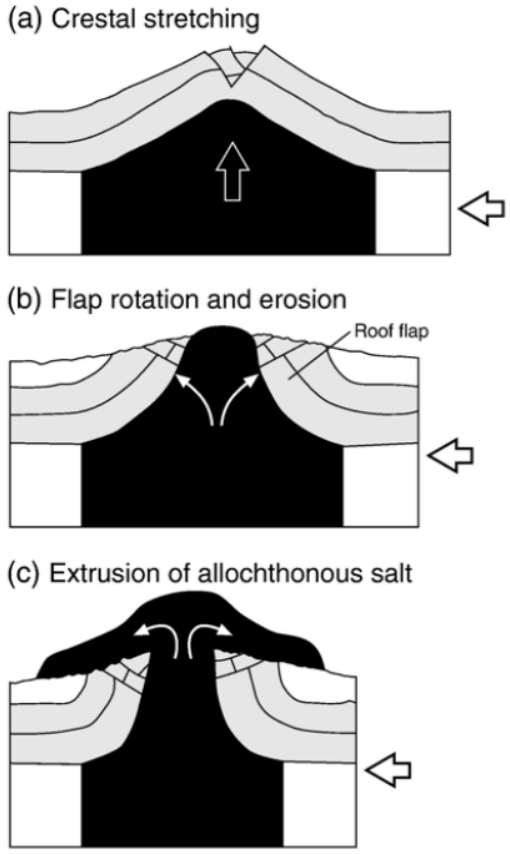

Figure 1: Example of a salt dome formation (diapir piercement) generated by compressional forces (regional shortening). This example assumes a pre-existing salt diapir, which is the most common scenario for piercement during shortening. Diapirs do not always progress through all these stages; whether or not they do depends on the magnitude of the shortening and the roof thickness above the diapir. (a) Arching of the diapir roof produces outer-arc extension, thinning, and weakening the roof. (b) The combination of a weakened roof and salt pressurized by lateral squeezing initiates the upward salt flow. Salt breaks through the thinned crest of the anticline, and the roof flaps on either side rotate away from the emerged diapir. (c) Rapid extrusion; salt displaced from the squeezed feeder flows out over the surface to form a salt glacier. Figures and captions from Hudec and Jackson (2007). [**NR**]

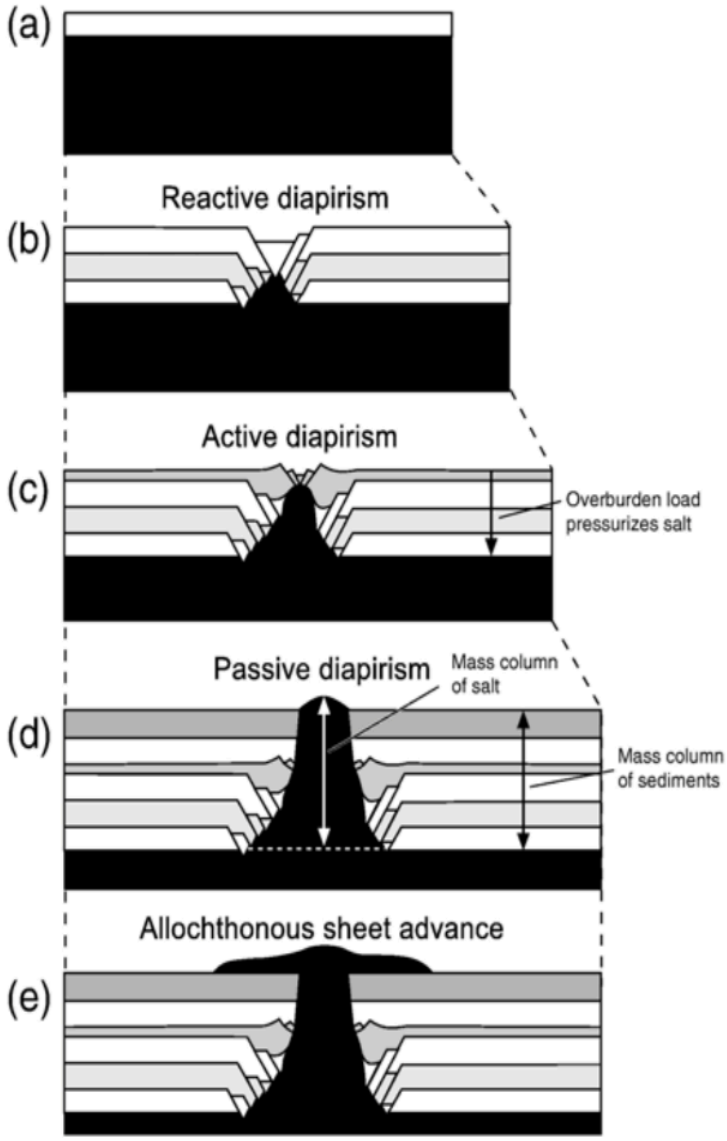

Figure 2: Example of a salt dome formation (diapir piercement) during regional extension. Diapirs do not necessarily progress through all these stages. The maturity of a given structure depends on the availability of salt, total amount of extension, and relative rates of extension and sedimentation. Figures and captions from Hudec and Jackson (2007). [**NR**]

Once this upward salt movement begins, salt from elsewhere in the salt bed moves into the region surrounding the salt plug to replace the salt that is flowing upward. The upward movement of the salt plug (or salt dome) continues as long as there is a sufficient source of salt feeding the dome or until the upward movement is halted by a more rigid formation (Figure 3). Once equilibrium is reached, upward movement of the salt dome ceases, but may begin again if sufficient sediments are added to the weight of the overburden which again increases the load pressure on the parent salt mass (King, 2015).

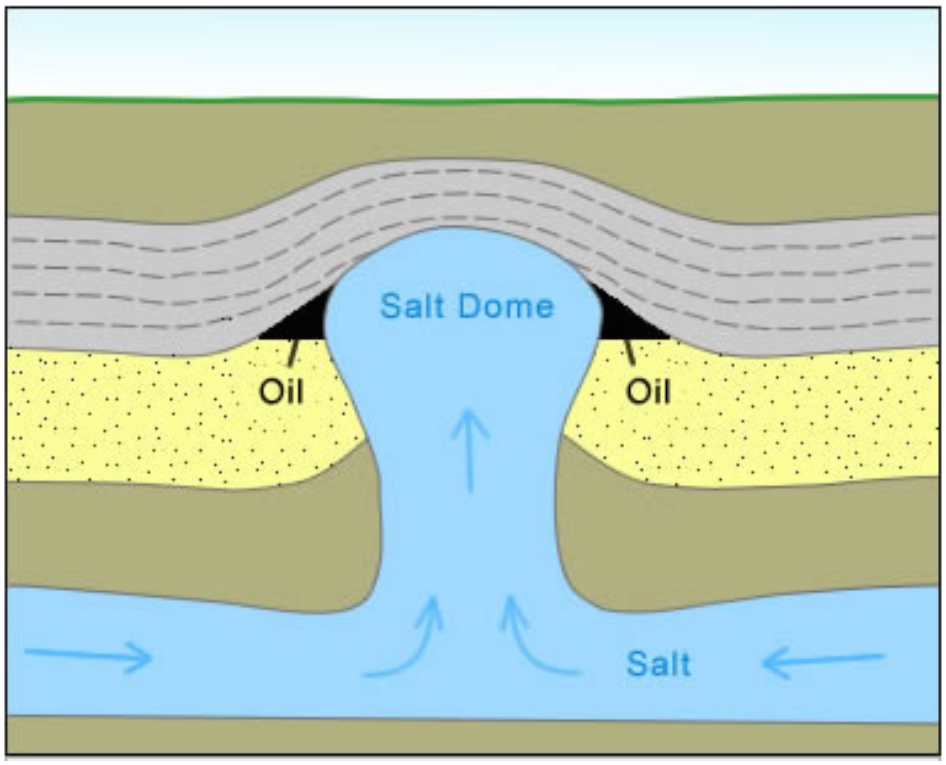

Figure 3: Schematic of the upward movement of the salt creating a salt dome. A salt dome is a type of structural dome formed when a thick bed of evaporite minerals (mainly salt or halite) intrudes vertically into surrounding rock strata, forming a diapir (defined as a mass of salt that has flowed ductilely and appears to have pierced or intruded the overburden). Figure and captions from King (2015). [**NR**]

Salt bodies play an important role in the entrapment of oil and gas. First, their cap rock can serve as an oil or gas natural reservoir. Moreover, when salt flows toward the surface, the rocks that it penetrates are arched upwards along the sides of the dome, and faults might be created. This deformation may allow oil and gas to migrate towards the salt dome where it can accumulate in a structural trap, because salt also acts as a seal to fluid migration (Figures 3 and 4). Until relatively recently, energy companies did not search for prospects underneath salt bodies because of poor-quality subsalt seismic data, and because they believed that reservoir-quality rock or hydrocarbons did not exist below salt layers. Advances in seismic processing,

imaging, and compelling drilling results from exploration wells encouraged companies to generate and drill prospects below salt layers, salt sheets, and other previously disregarded potential traps (Schlumberger, 2015). Therefore, a single salt body/dome can have many associated reservoirs at a variety of depths and locations in its vicinity.

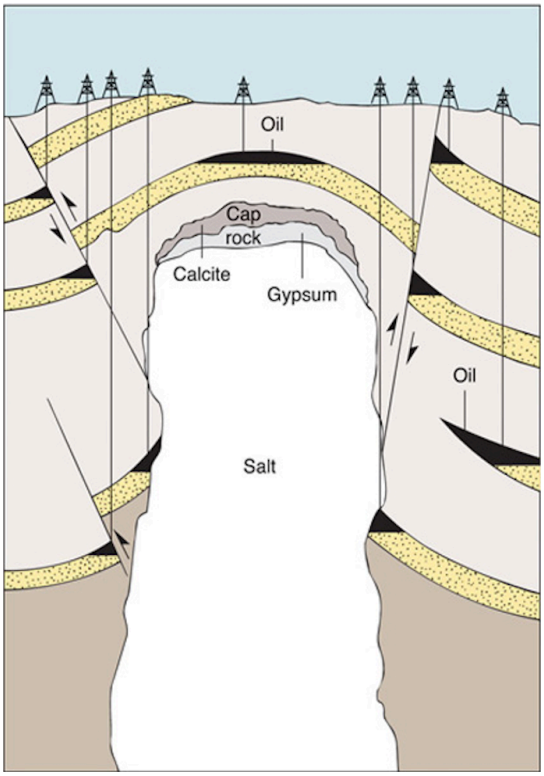

Figure 4: Salt dome, illustrating how the rising salt causes the surrounding sedimentary layers to be arched up, forming areas in which hydrocarbons might accumulate. Figure and captions from Levin (2009). [**NR**]

Though potentially very rewarding, drilling through salt can be challenging, costly, and risky. Drillers have to address factors that cause openhole instability and accompanying problems, including borehole walls weakened by incompatible muds, restrictions and an undergauge hole caused by salt creep; or an enlargement caused by dissolution. Moreover, the actual salt rock is weak and undergoes continuous deformation. During the life of a well, salt movement can displace wellbore tubulars, possibly causing failure or restricted access (Farmer et al., 1996). Therefore, obtaining well-focused images of subsalt potential reservoirs is extremely important for risk assessment, as well as for the decision-making process.

Geophysical properties of salt bodies

Leveille et al. (2011) provide a description of a typical geophysical setup that one should expect when exploring a zone containing salt bodies. The salt dome is usually

a thick salt sheet (1 to 5 km), with a very rugose top and a relatively smooth base with potential sharp discontinuities coming either from the suturing of two or more salt bodies or from normal faulting. The sediments at the top of the salt sheet are much younger than the salt, while the deeper (i.e., subsalt sediments) can be of any age. The flank of the salt dome is usually very steep (Figures 4 and 5). Pure salt P-wave velocity is typically 4,500 m/s, with a V_p/V_s ratio of 1.9, and a mass density of 2.16 g/cm^3. Salt is extremely light and very fast acoustically. For comparison, a shale with the same P-wave velocity would have a mass density of approximately 2.65 g/cm^3. Near the top of the salt, one should expect younger sediments; with P-wave velocities of approximately 2,000 m/s near the sea floor, and possibly up to 3,000 m/s near the top of the salt. Near the base of the salt, the range is from 3,000 m/s to as high as 4,000 to 4,500 m/s. Moreover, it is common to have highly overpressured sediments near the base of the salt, which can have velocities even lower than 3,000 m/s.

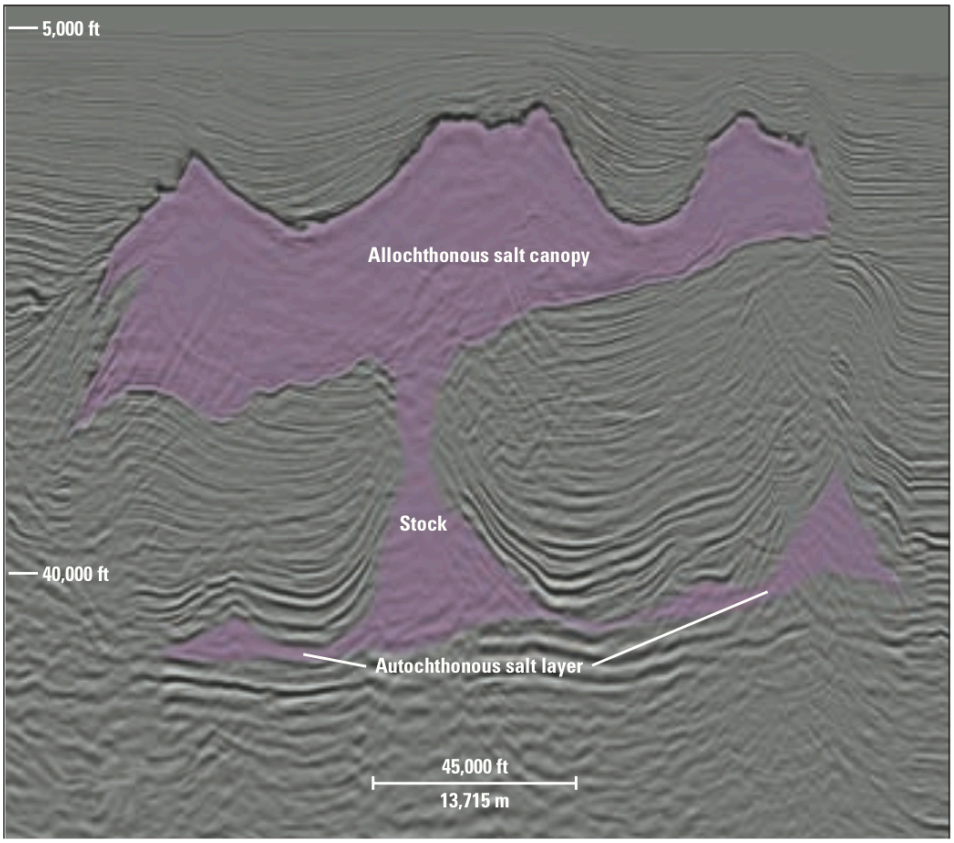

Figure 5: Interpreted seismic section of a salt body beneath the Continental Slope off Louisiana. This figure shows the evolving salt structure. Figure and captions from Dribus et al. (2008). [**NR**]

Challenges of seismic imaging in the vicinity of salt bodies

From available literature, we identified six major reasons why seismic imaging in the presence of salt bodies is a challenge (Leveille et al. (2011); Ritter et al. (2010); Jones and Davison (2014)).

1. The main physical problem with the presence of thick allochthonous salt sheets surrounded by acoustic softer sediments is an illumination issue related to the geometry of the sediment-salt interface. Because of the strong acoustic impedance and velocity contrast between the sediments and the salt, the critical angles between sediments and salt are greatly decreased (approximately 20 to 30 degrees when the top-salt is near the seafloor). Therefore, the energy from a shot is rapidly defocused as it passes through the salt and travels down the base. Only a fraction of the incident energy arrives at a subsalt reflector. Moreover, the subsalt energy that is reflected becomes subject to another critical effect barrier (i.e., the critical angle between subsalt sediments and salt) on its way upward, which can sometimes make certain reflector geometries impossible to image from various directions (such as a reflector dipping at the critical angle relative to the salt base). Variability in the salt-interface geometry, especially rapid variability, causes defocusing of the raypaths, thereby producing holes in the illumination pattern subsalt. These holes are dependent on the local geometry of the salt surface, and therefore can vary rapidly with the azimuths of the raypaths (this effect has been used to attempt to fill in the illumination holes by finding potential azimuths where the holes do not exist). It is often stated that the salt acts as a partial "mirror," which is commonly misinterpreted to mean that the salt causes the energy losses simply by reflection/transmission losses, but it is not the case (Leveille et al., 2011).

2. The interpretation and the adjusting of fine-scale details around the salt boundaries can be very challenging and tedious. A small error in the positioning of this interface the can have severe consequences and distort the image-quality of underlying subsurface features. This issue is the main focus of our future research and we discuss it into more detail in the next section.

3. Subsalt reflectors are in general very weak reflectors, with reflection coefficients in the 5% range; at least for a large portion of the subsalt projects in the Gulf of Mexico (Leveille et al., 2011).

4. On top of having a strong acoustic impedance contrast with its surrounding sediments, salt bodies and diapirs may also have very complex geometrical shapes (e.g., steeply dipping and overturned flanks), which makes the travelpaths of seismic waves in the vicinity of salt bodies very complicated to model and to interpret. Therefore, it requires the use of costly imaging algorithms (e.g., two-way wave-equation engines that can model double bounces and turning wave reflections).

5. When a salt body moves, the presence of dirty salts can entrain sediments with it. These sediments can get trapped between two colliding salt sheets (referred to as "sutures"). There can be several sutures within what looks like a large continuous salt body. The result is that allochthonous salt sheets can vary in composition, from more or less pure salt (referred to as "dirty salt") containing trapped sediments, usually shale material. The composition and the seismic velocity of the material trapped in the sutures can vary widely, which makes it challenging to model accurately.

6. Lack of anisotropy representation and parametrization within a salt body: most of the time, there is not sufficient information to describe the anisotropic behavior inside salt bodies. But, all deformed salt bodies contain interbeds of different compositions and mineral grains, which are elongated in the salt flow direction (Hudec and Jackson, 2007). The direction is roughly vertical in salt diapirs, and parallel to strata in autochthonous layers (salt bed or layer located in the emplacement where it was originally deposited). An ultrasonic P-wave velocity anisotropy (wavelength less than 1 mm) has already been measured at up to 7% faster in the flow direction (Jones and Davison, 2014). However, to date, there has been little attempt to incorporate salt anisotropy into velocity model building.

CHALLENGES SPECIFIC TO TOP-SALT DELINEATION

Even with today's best seismic imaging algorithms, such as migration velocity analysis (MVA), full-waveform inversion (FWI), and tomographic full-waveform inversion (TFWI), the very rugose geometry of the sediment-salt interface is difficult to model and delineate accurately to the scale needed to obtain high-quality images of subsalt reflectors. We analyze in this section why current algorithms may still fail to provide a high-resolution image of the boundary. From available literature, we identified four challenges that could explain the limitations of our current algorithms.

Complex transition zone

The transition between younger overlying sediments and the rock salt is rarely as clean as we may think. During the formation of salt domes or salt bodies, large blocks of sediments (referred to as "rafts" or "carapaces") can ride on top of the moving salt. These carapaces, usually shales or carbonates, can sit on the salt and be interposed between the younger overlying sediments and the top-salt. They are made of older sediments that have a very high density, velocity, and velocity range (more than 4,500 m/s). This wide velocity range is primarily influenced by other post-depositional, diagenetic processes, and not just by pure compaction at increasing burial (Anselmetti and Eberli, 1993; Leveille et al., 2011). Carbonate carapace layers are usually not very thick (up to several hundreds of meters (Leveille et al., 2011)), and are very common

in the Gulf of Mexico. They generally have a velocity relatively close to salt, which means that they can negate the impedance contrast that usually marks the sediment-salt boundary (Ritter et al., 2010). In fact, the expected impedance contrast is often seen somewhere within the carapace and may lead to misinterpretation of the top-salt. An incorrect interpretation may create a distortion in the subsalt events caused by the misplacement of the top of salt and too slow overlying sediment velocities (Ritter et al., 2010). In some cases, it is also possible to have a reflection from the carapace-salt interface generated by a pure density contrast. Because most of the current seismic imaging algorithms assume a constant density Earth, they would not be able to accurately model these reflections.

Figure 6 shows a set of three well logs from two different wells drilled into the same salt body in the Gulf of Mexico (the red and green logs come from the same well). On the blue log (sonic P-wave velocity), a clear interface is visible at a relative depth of 300 m, but we can also identify an intermediate zone, which can be interpreted as a carapace, with a thickness of approximately 150 m interposed between the bottom of the sediments, and the top of the salt. This log illustrates the issue stemming from the existence of a transition zone between the young uncompacted sediments and the salt rock. In this case, an interpreter could identify the interface between the sediments and the carapace as the top-salt, and assign an inappropriate (too-low) velocity value to the few 100 meters of the carapace layer. The base salt interface, however, appears a lot cleaner. As expected, the subsalt sediments have a lower P-wave velocity (red curve) than the actual salt, but are denser (green curve). It is also important to notice that the salt sonic P-wave velocity appears to be higher in average on the red curve, which may indicate some compaction effect within the salt body.

Another potential difficulty can arise from the fact that many buried salt diapirs have a cap rock. It is a carapace of anhydrite, gypsum, and limestone (in ascending order) immediately above the salt rock of a salt dome (Figures 7(a) and (b)). The average cap rock is between 100 m to 150 m thick, but can be as thick as 300 m. It is a secondary product created as the salt dome ascends through the overlying materials. The top of the dome dissolves as it rises through the sediments and the material constituents of the salt become concentrated at the top of the rising plug becoming three layers. The cap rock of some salt domes, and sometimes the actual rock salt, is found to overhang, or drape down the sides of the main salt mass, as shown in Figure 7(c). Salt is soluble and dissolves, but the cap rock is not very soluble and thereby left more intact. Thus the appearance of the cap rock overhanging the main salt body is the result of dissolution of the salt body within the subsurface, but not dissolving the cap rock. The presence of a cap rock may makes the sediment-salt interface difficult to accurately delineate.

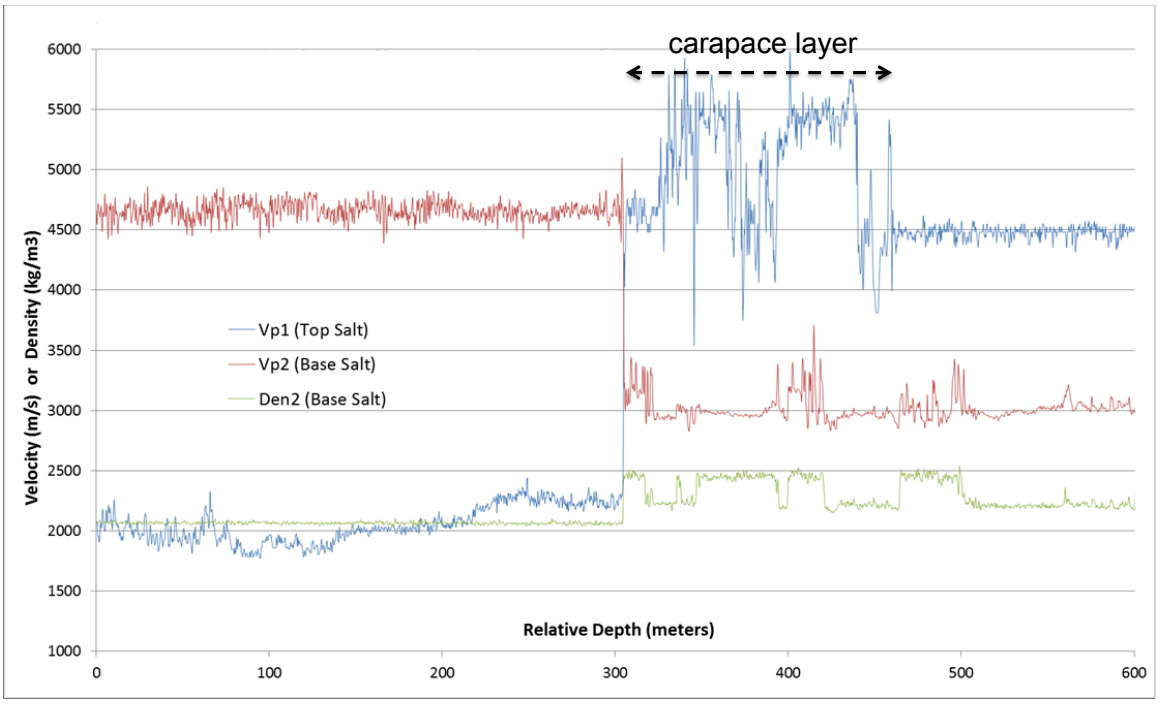

Figure 6: Well logs from one salt body in the Gulf of Mexico. The blue curve shows the sonic log for the P-wave velocity above and below the top-salt interface as a function of relative depth (the top-salt interface has been shifted to a relative depth of 300 m for proprietary reasons). The red curve shows the sonic log for P-wave velocity above and below the base-salt interface as a function of relative depth (the base-salt interface has also been shifted to a relative depth of 300 m). The green curve shows the density log around the base salt as a function of relative depth, and comes from the same well as the one for the red curve. The blue log comes from a different well. The wells were drilled from the same platform into the same salt body, but at different penetration points. Courtesy of Chevron Corporation. [**NR**]

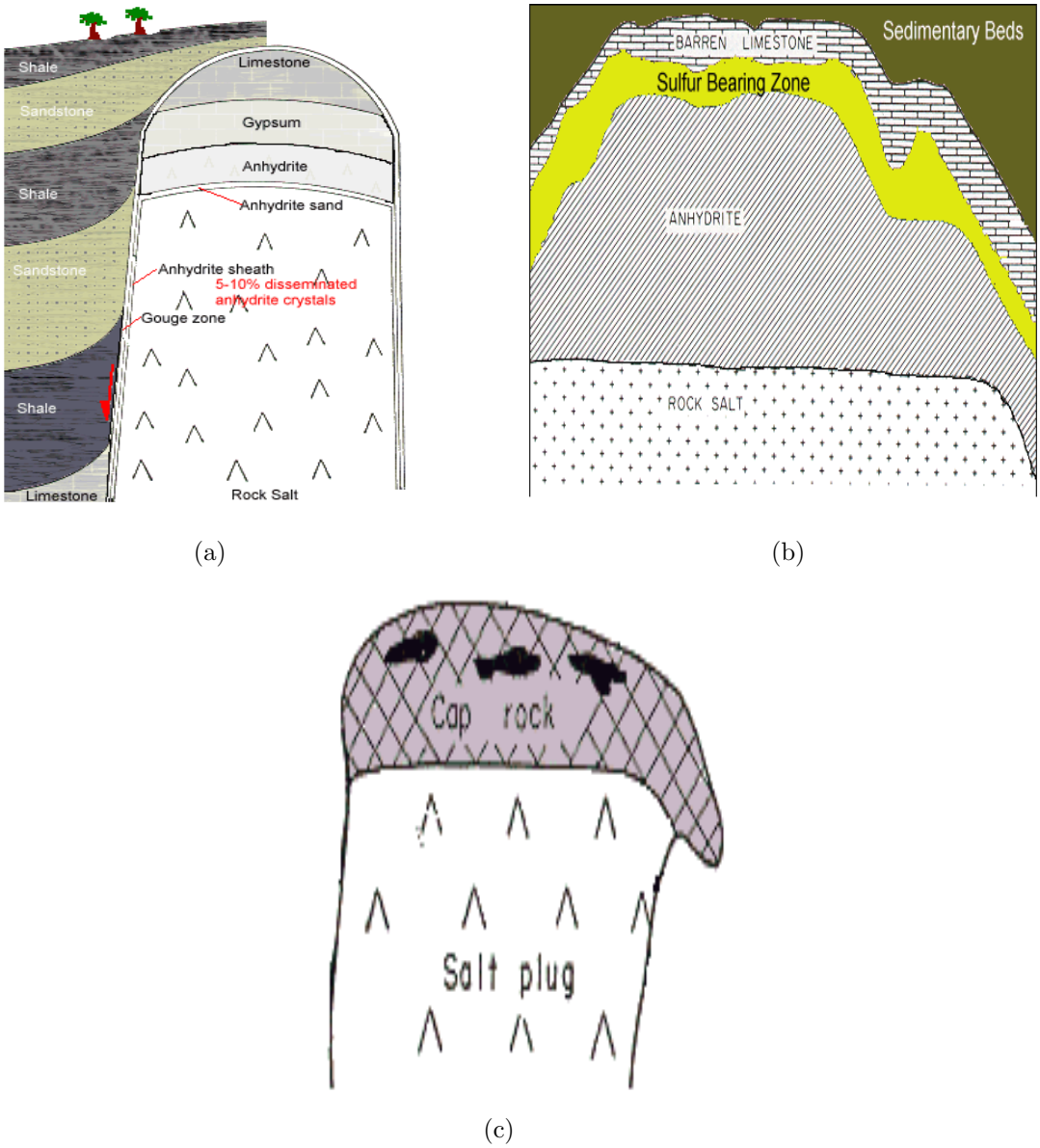

Figure 7: Schematic illustration of salt cap rocks. (a) The cap is composed of limestone located at the top of the dome followed by, in descending order, gypsum, anhydrite, and finally rock salt. (b) Cap rock has all the characteristics of a petroleum reservoir and often contains hydrocarbons. But cap rock also contains sulfur (i.e., gyspum) that is present in the cap rocks of almost all salt domes. The sulfur forms after the limestone is created and is derived from the destruction of the anhydrite. (c) The cap rock of some salt domes is found to overhang or drape down the side of the main salt mass. It is commonly found to overhang on one or two sides. Figures and captions from DNR (2015). [**NR**]

Inaccurate velocity model of the overburden

To correctly image the top-salt, a very precise overburden velocity model is needed. Typically, a FWI inversion scheme could be used to build such a model. However, if the top-salt is buried too deeply into the subsurface, or if recorded data lack transmitted or refracted low-frequency energy, the inversion scheme might fail to deliver an accurate overburden velocity model down to the top of the salt.

Tortuous top-salt geometrical shapes

Current algorithms may fail to get an ideal image of what the top-salt is because of the complex geometry of certain salt bodies. Figures 8(a) and (b) show two cross-sections of a velocity model from the Gulf of Mexico wide-azimuth "E-Octopus" dataset, and illustrate the type of top-salt shapes encountered in salt basins. The circled zones are challenging to model accurately, even with a long-offset and wide-azimuth acquisition.

Lack of good-quality high-frequency data

Current algorithms can be limited by the low signal to noise ratio for higher frequencies contained in the data. This limitation may set an upper bound on the resolution of our inverted velocity model that may be too low to recover some of the fine-scale features of the top-salt interface.

EFFECTS OF INACCURATE TOP-SALT DELINEATION ON WAVEFIELDS

As shown in recent work (Etgen et al., 2014a,b; Albertin et al., 2014), misinterpreting the top-salt boundary can deteriorate the images of underlying layers. In this section, we illustrate the effect of a top-salt misinterpretation by looking at the actual wavefields. We propose two scenarios; one when the true top of the salt body is relatively smooth, and one when the true top-salt is rugose. We simulate a seismic reflection experiment in which we place a single source at a depth $z_s = 0$ m, a horizontal position $x_s = 500$ m, and 600 geophones equally spaced along the horizontal axis, at a depth $z_r = 0$ m. The reflector we try to image is located at a depth $z_{ref} = 4.7$ km. We perform a partial migration using a single shot, and a two-way wave-equation acoustic and isotropic engine. As we purposely decrease the accuracy of the top-salt picking, we analyze the change in behavior of the back-propagated receiver wavefield and the partially migrated images.

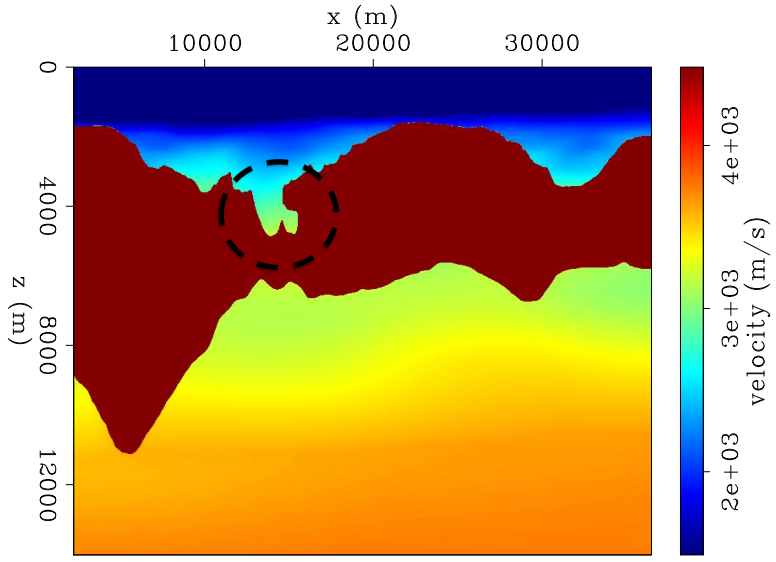

(a)

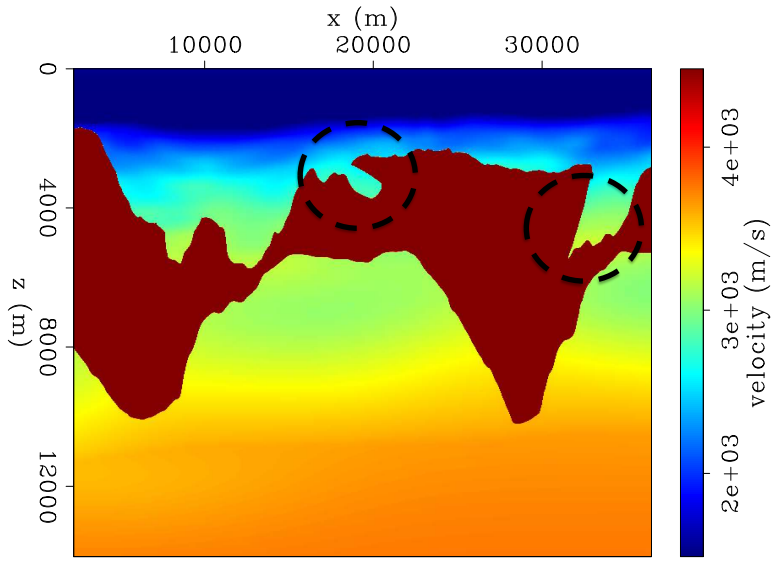

(b)

Figure 8: Cross-sections from E-Octopus data set (Gulf of Mexico) displaying the tortuosity of the top of salt bodies. Circled areas may suffer from a lack of illumination and are challenging to model accurately. Courtesy of WesternGeco. [**NR**]

Smooth top-salt

Figures 9(a)-(d) show the true model, true background, inaccurate background (i.e., the background with a misinterpreted top-salt), and difference between the true and the incorrect backgrounds, respectively. Figure 10 (left and right columns) show three snapshots of the receiver wavefields back-propagated in time, and computed with the two different background models. The left column shows the wavefield computed with the correct background model. The receiver wavefield is then cross-correlated in time with the source wavefield to generate a partially migrated image (Figure 11(a)). The right column of Figure 10 shows the receiver wavefield computed with the inaccurate background model. The contribution of this shot to the migrated image is displayed in Figure 11(b). Even though the inaccuracy of the top-salt affects the behavior and the shape of the receiver wavefield, it does not damage it considerably. The partial image in Figure 11(b) is distorted, but it will likely be possible to improve the fully migrated image (i.e., the image generated with more shots) by applying a tomographic optimzation scheme (e.g., WEMVA).

Rugose top salt

In this test, the true top-salt boundary is rugose. Figures 12(a)-(d) show the true model, true background, inaccurate background (i.e., the model with the misinterpreted top-salt), and difference between the true and the incorrect backgrounds, respectively. Figure 13 (left column) shows three snapshots of the receiver wavefield computed with the correct background model, while Figure 13 (right column) displays the receiver wavefield computed with the inaccurate background. We see two major differences from the previous case.

Firstly, we notice that the receiver wavefield has a much more complex shape, especially at later physical times (Figures 13(a) and (b)), which is because the wavefield that illuminates the reflector propagates twice through the rugose top-salt before it is recorded at the surface.

Moreover, we can see that in Figures 13(c) and (e) the back-propagated receiver wavefield computed with the accurate top-salt has been well refocused: its wavefront is much smoother than it is at later physical times (Figure 13(a)). During the back-propagation of the receiver wavefield through the rugose top-salt, the fine-scale features of the salt boundary behave as point scatterers. Because we are using the correct top-salt, they collapse and remove most of the diffraction artifacts present in the wavefield at later physical times (Figure 13(a)). The partially migrated image from this shot (Figure14(a)) is accurate. However, in the case of a misinterpreted top-salt, the receiver wavefield does not refocus properly. The back-propagation through the inaccurate salt boundary creates even more asynchronized scattering (Figures 13(d) and (f)). Consequently, the partially migrated image is considerably damaged (Figure14(b)), and the image degradation is much more pronounced than in the previous example (Figure11(b)).

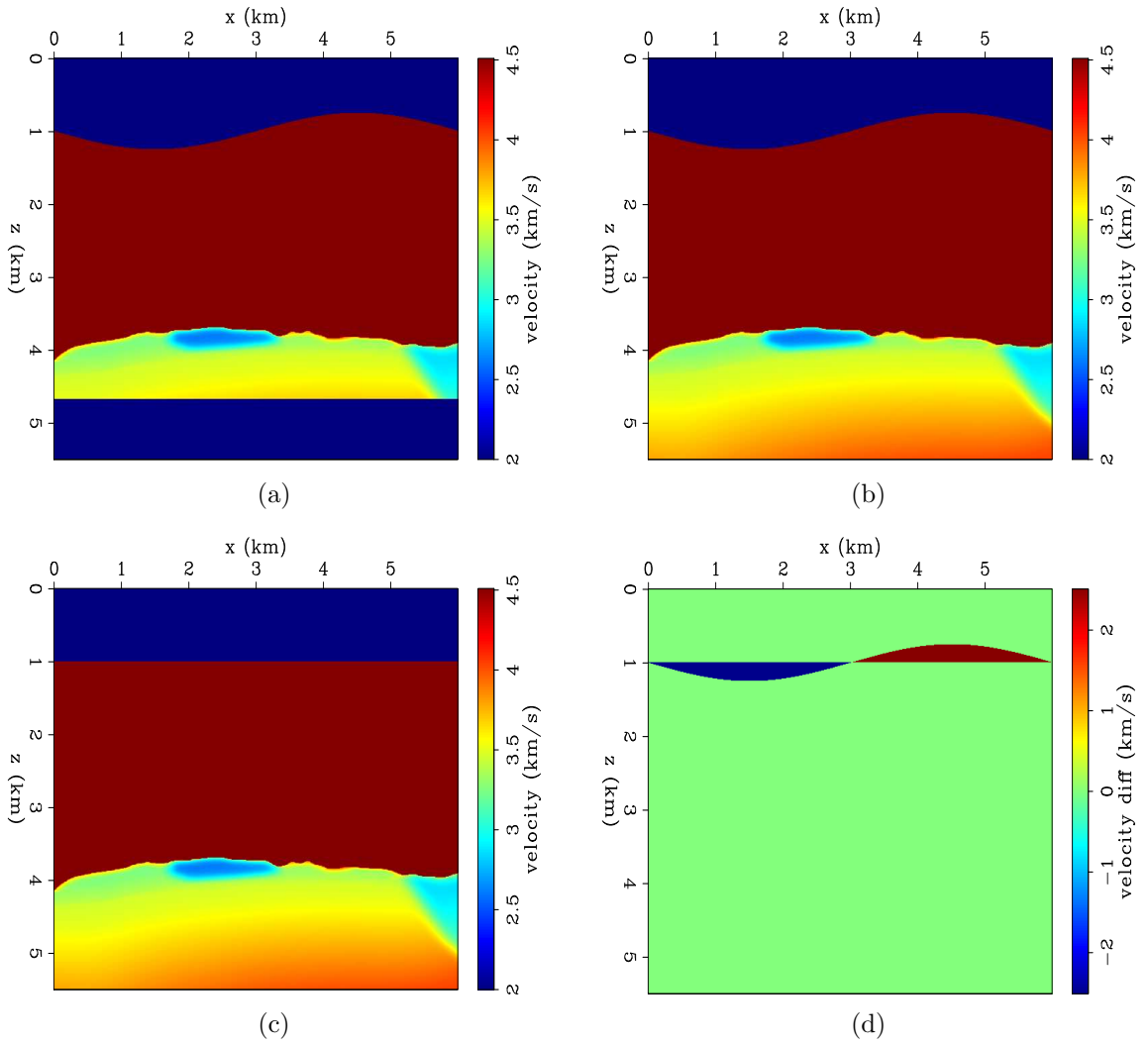

Figure 9: Synthetic velocity models, modified from the 2004 EAGE velocity benchmark study. (a) True velocity model. (b) True background velocity model. (c) Inaccurate background velocity model. (d) Difference between true background and inaccurate background velocity models. [**ER**]

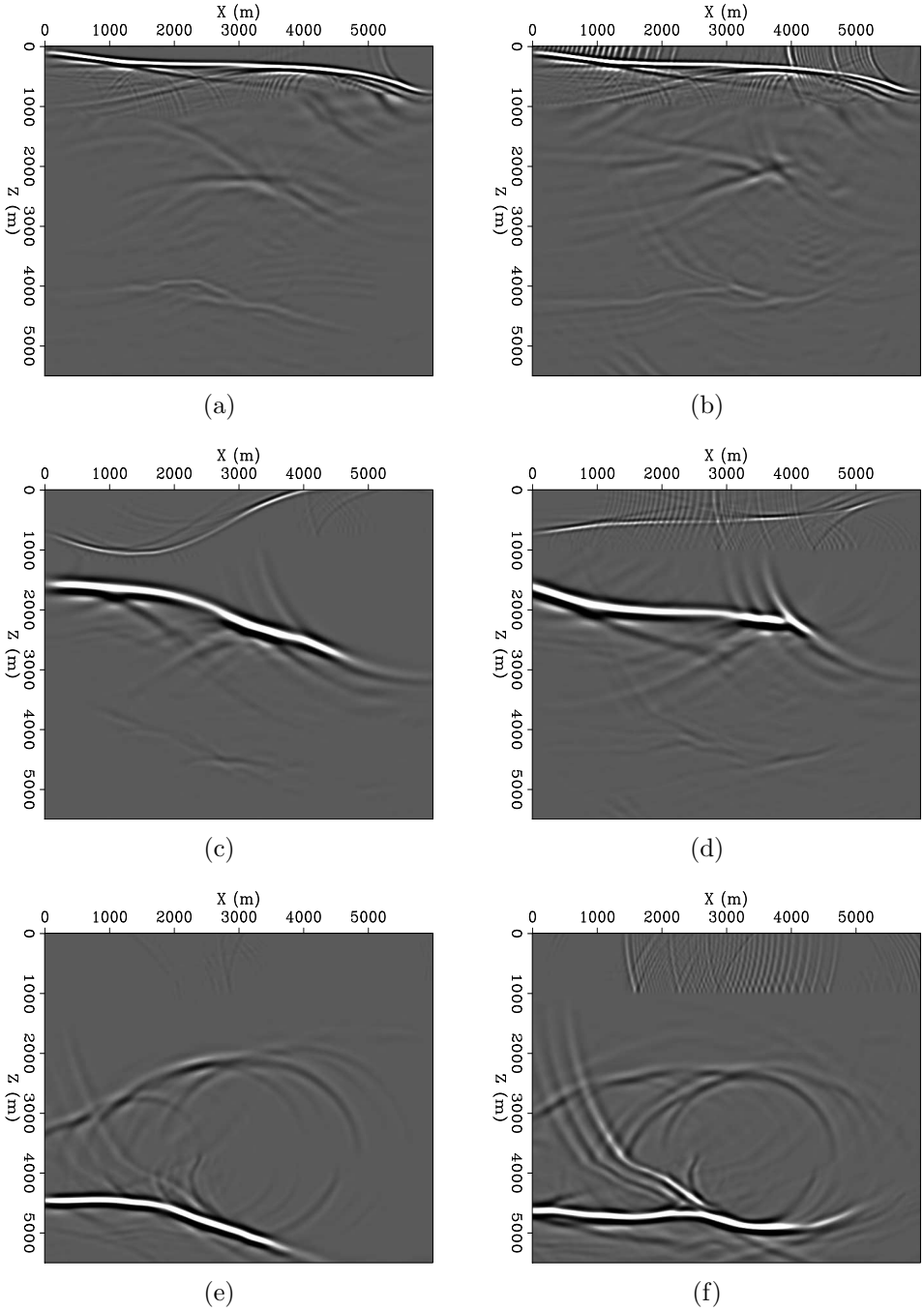

Figure 10: Snapshots of two receiver wavefields. Left column shows three snapshots of the receiver wavefield computed with the true background velocity model. Right column shows three snapshots of the receiver wavefield computed with the inaccurate background velocity model. Snaphots in first row are computed at $t_3 = 2.784$ s. Snapshots in second row are computed at $t_2 = 2.208$ s. Snapshots in last row are computed at $t_1 = 1.536$ s. [**ER**]

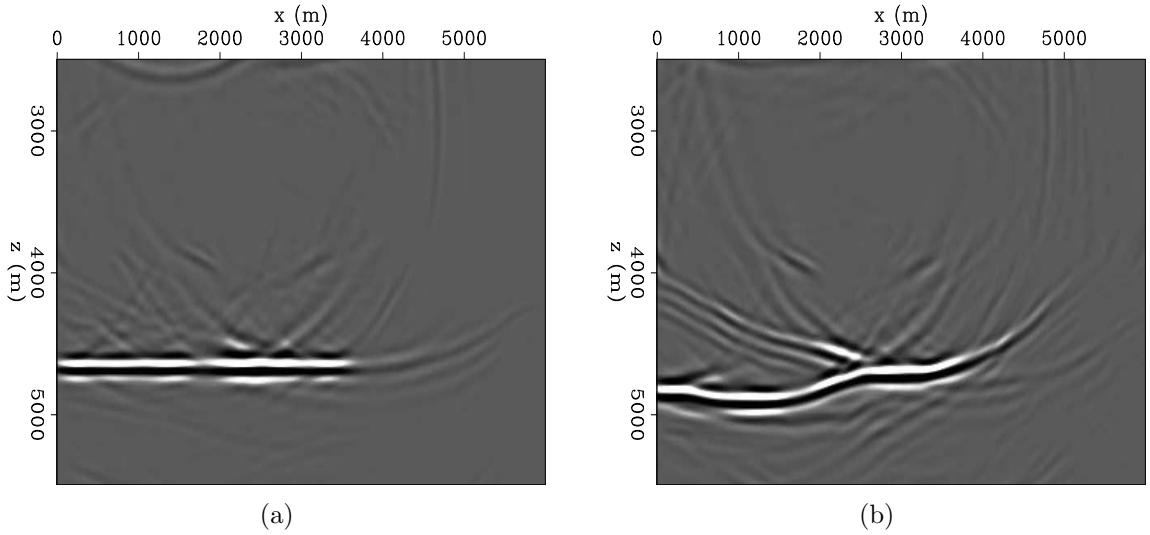

(a) (b)

Figure 11: Partially migrated sections (one shot) using a two-way wave-equation engine. (a) Partial image computed using the true background velocity model. (b) Partial image computed using the inaccurate background velocity model. [**ER**]

DEGRADATION OF SUBSALT REFLECTORS IMAGE QUALITY

We conduct three noise-free synthetic tests to illustrate the degradation of subsalt layer images when using an inaccurate top-salt model to migrate data. Computations are performed using a two-way wave-equation engine. We use a 25 Hz Ricker wavelet for the source function. Migrated images are generated with 100 sources located at the surface, and equally spaced along the horizontal axis. We set geophones at the surface at every grid point. Images are extended along the horizontal subsurface offset axis, and then converted to subsurface angle domain by a slant-stack operator.

Single flat layer

We perform two migrations with two different background velocity models. Our goal is to image the reflector at $z = 3,500$ m, and see how its image deteriorates with decreasing accuracy of the background model. Figure 15(a) shows the true model used to generate the synthetic data, while Figures 15(b) and (c) show the two different background velocity models used to image the subsalt reflector. Figure 15(d) shows the difference between the inaccurate background and the true background velocity model. The results of the migrated layer are shown in Figure 16(a) and (b). In Figure 16(b), we can see that the misinterpretation of the top-salt has damaged the image of the layer. The reflector shows a strong lack of lateral continuity, and its shape is highly distorted. Moreover, the angle gathers do not provide any coherent moveout information (Figures 17 and 18).

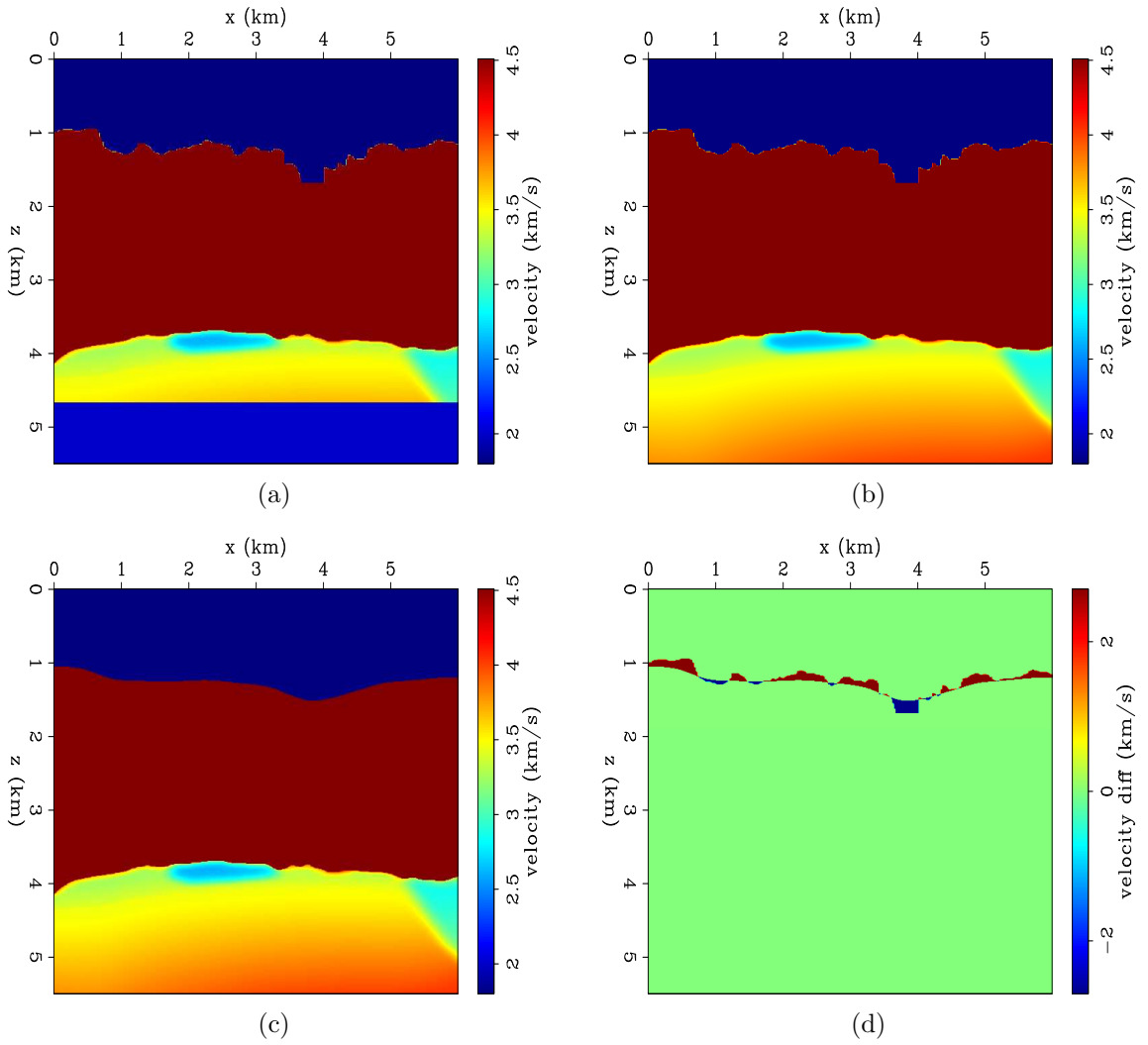

Figure 12: Synthetic velocity models, modified from the 2004 BP synthetic model. (a) True velocity model with a rugose top-salt. (b) True background velocity model. (c) Inaccurate background velocity model. (d) Difference between true background and inaccurate background velocity models. [**ER**]

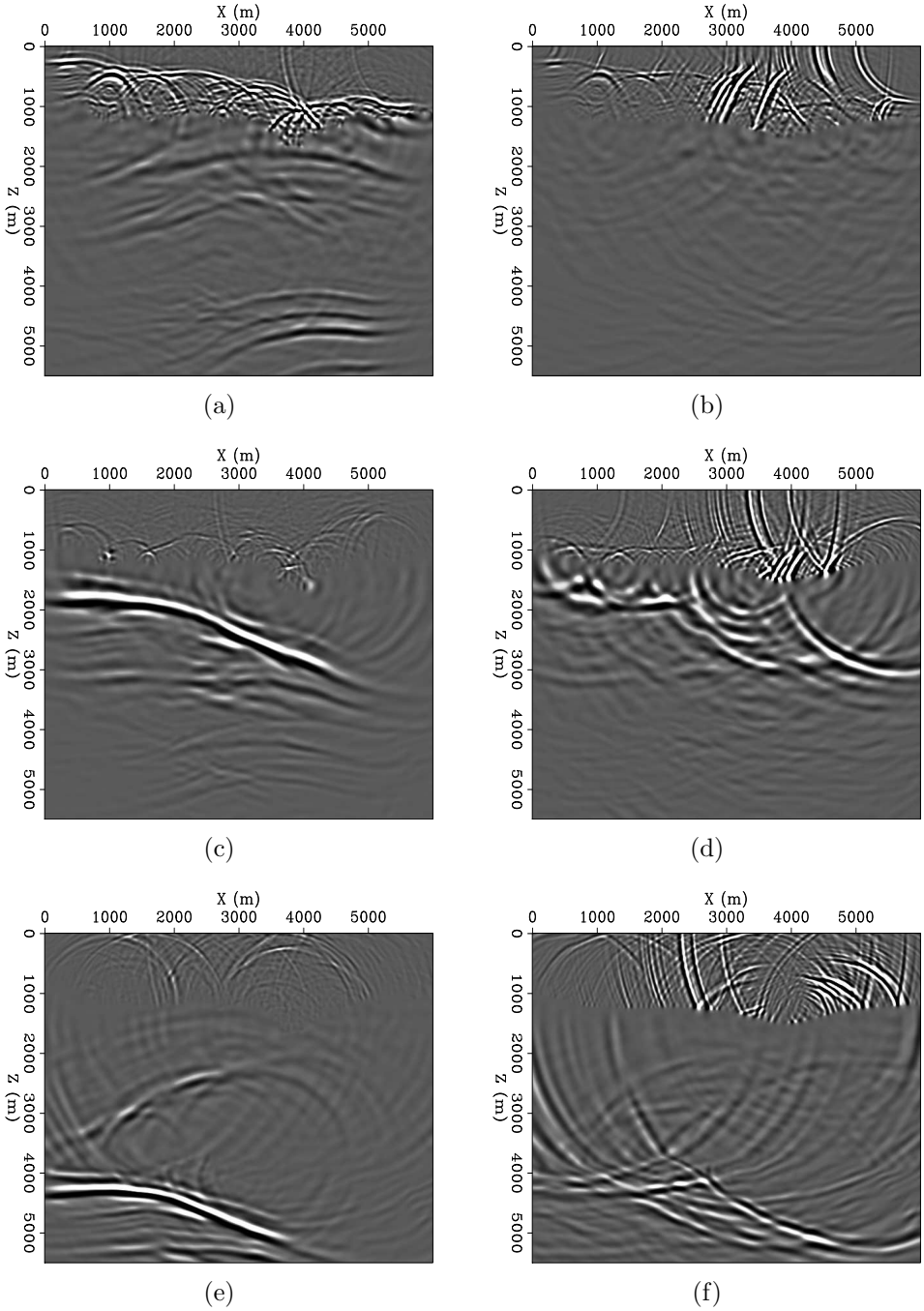

Figure 13: Snapshots of two receiver wavefields. Left column shows three snapshots of the receiver wavefield computed with the true background velocity model. Right column shows three snapshots of the receiver wavefield computed with the inaccurate background velocity model. Snapshots in first row are computed at $t_3 = 2.832$ s. Snapshots in second row are computed at $t_2 = 2.256$ s. Snpashots in last row is computed at $t_1 = 1.680$ s. [**ER**]

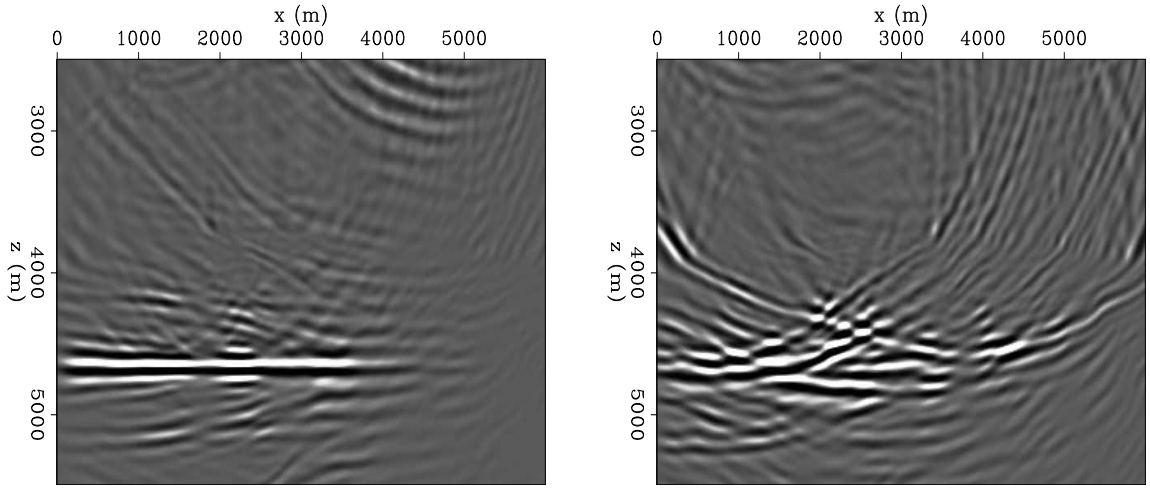

(a) (b)

Figure 14: Partially migrated sections (one shot) using a two-way wave-equation engine. The true velocity model contains a salt body with a rugose top-salt. (a) Partial image computed using the true background velocity model. (b) Partial image computed using the inaccurate background velocity model. [**ER**]

Sinusoidal-shape reflector

A similar experiment as described in the previous section is conducted, but the goal is to image a reflector with a sinusoidal shape. The velocity models are displayed in Figure 19. Figure 20 and shows the migrated images generated by an accurate top-salt model (Figure 20(a)), and an inaccurate top-salt (Figure 20(b)). Though the reflector image is degraded, it is still interpretable and relatively continuous. However, the angle gathers still show no coherency (Figures 21 and 22).

Multiple layers

The two previous examples showed image degradations even though the models had quite simple geometries. In this test, we include two strong reflectors below the base salt (Figure23(a)) to simulate a more complex scenario. Images in Figures 24(a) and Figures 24(b) are computed with the background velocity models displayed in Figure 23(b) and Figure 23(c), respectively. As expected, we see a degradation of the two subsalt layers, as well as the angle gathers (Figure 25 and 26) are not coherent.

Conlusions on synthetic tests

We performed synthetic tests to assess how images of subsalt layers are damaged with inaccurate top-salt delineation. By looking at the actual wavefields, we showed that

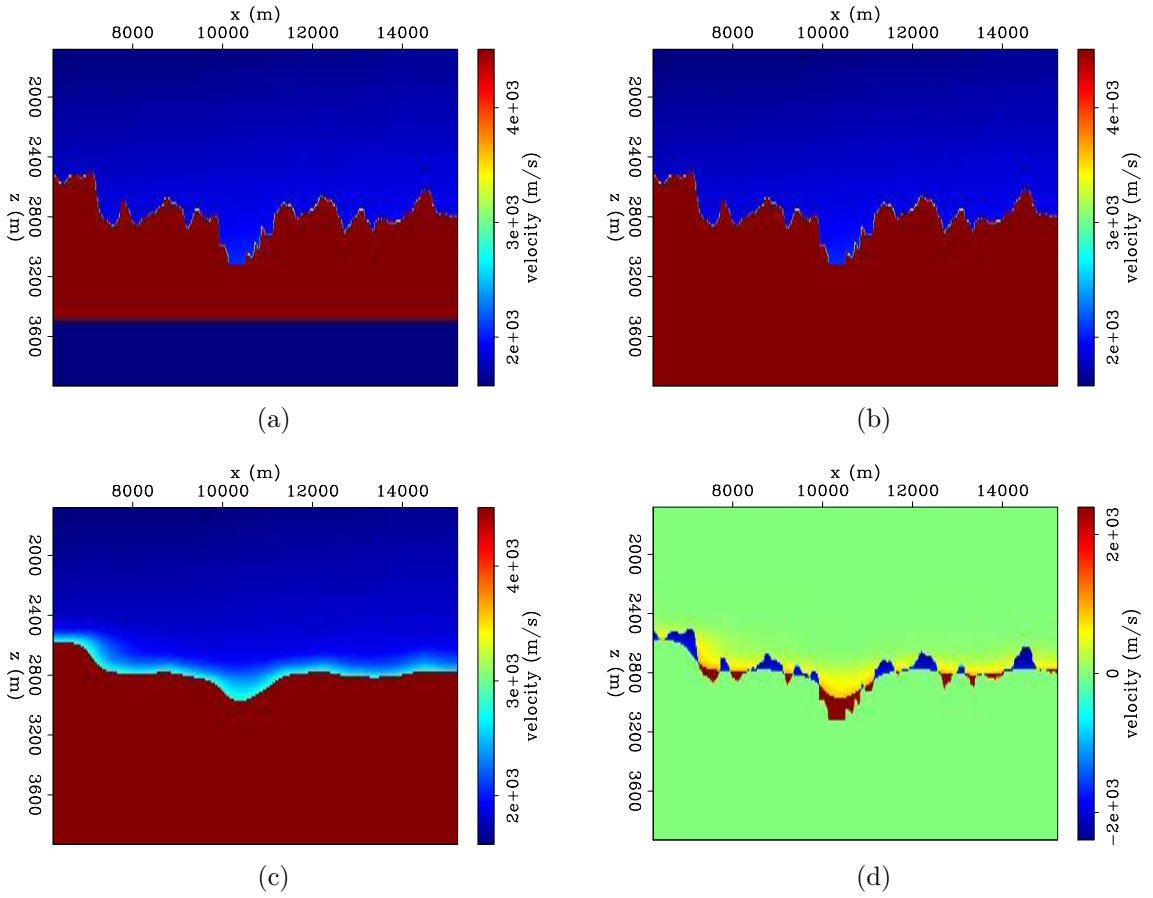

Figure 15: Velocity models modified from the the 2004 EAGE velocity benchmark study. (a) True velocity model. (b) True background velocity model. (c) Inaccurate background velocity model. (d) Difference between true and inaccurate background velocity models. [**ER**]

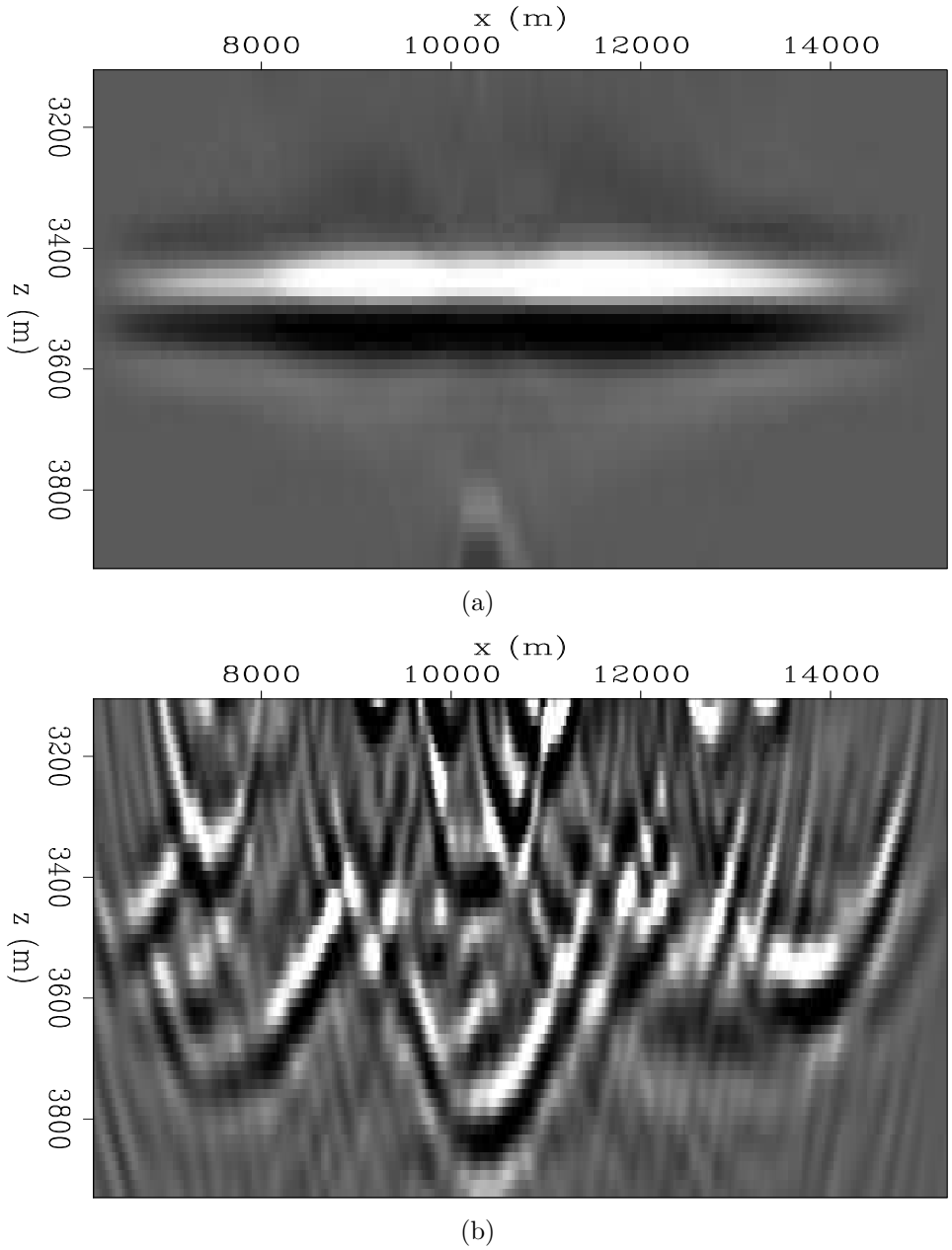

Figure 16: Migrated images of the subsalt reflector shown in Figure 15(a) using a two-way wave-equation engine. (a) Migrated layer using the true background velocity model. (b) Migrated layer using the inaccurate background velocity model. [**ER**]

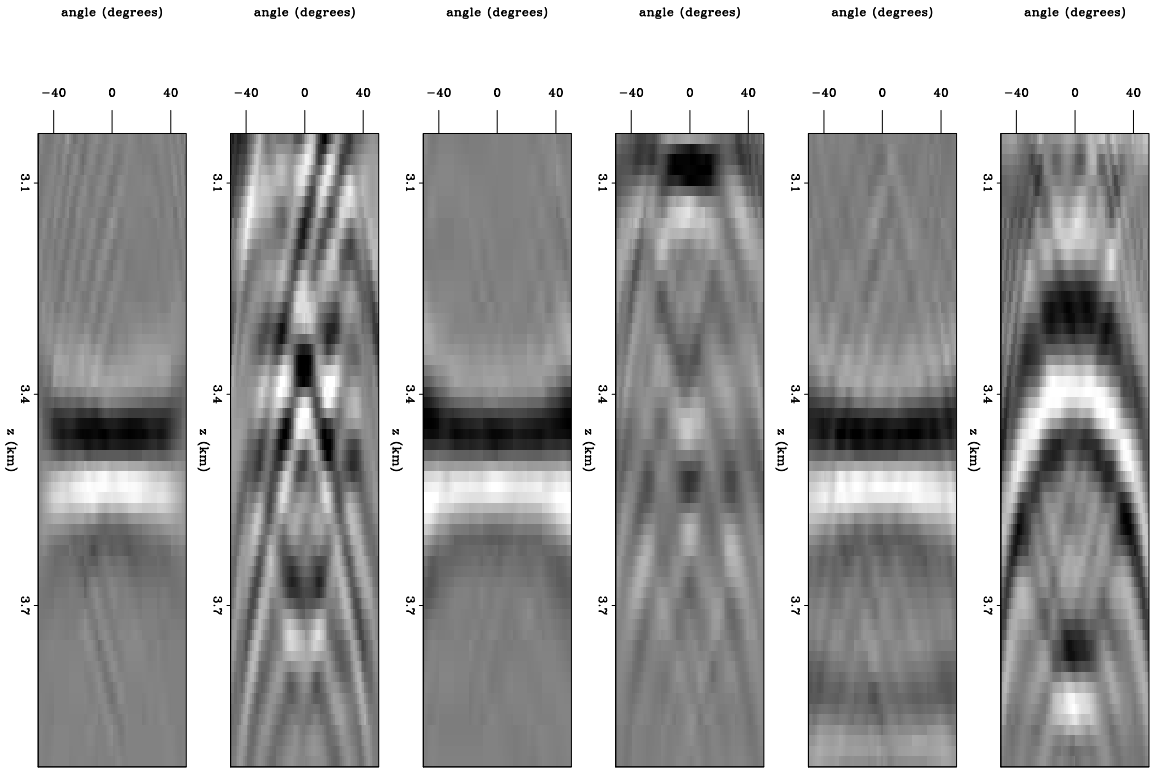

Figure 17: Three pairs of angle domain common image gathers (ADCIG). For each pair, the first image shows the gather computed from the accurate image (Figure 16(a)), and the second image shows the gather computed from the distorted image (Figure 16(b)). The gathers are computed at $x_1 = 7,617.5$ m, $x_2 = 9,177.5$ m, and $x_3 = 10,377.5$ m, respectively. [**ER**]

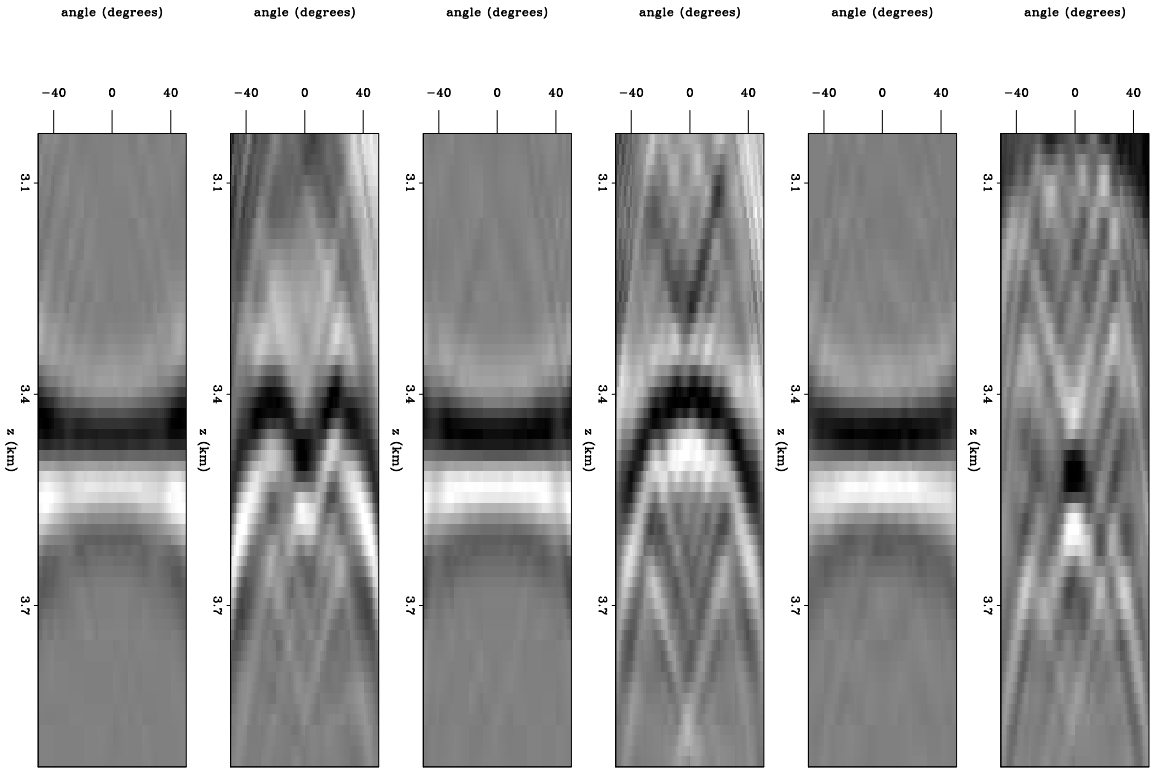

Figure 18: Three pairs of angle domain common image gathers. For each pair, the first image shows the gather computed from the accurate image (Figure 16(a)), and the second image shows the gather computed from the distorted image (Figure 16(b)). The gathers are computed at $x_4 = 11,352.5$ m, $x_5 = 12,267.5$ m, and $x_6 = 13,137.5$ m, respectively. [**ER**]

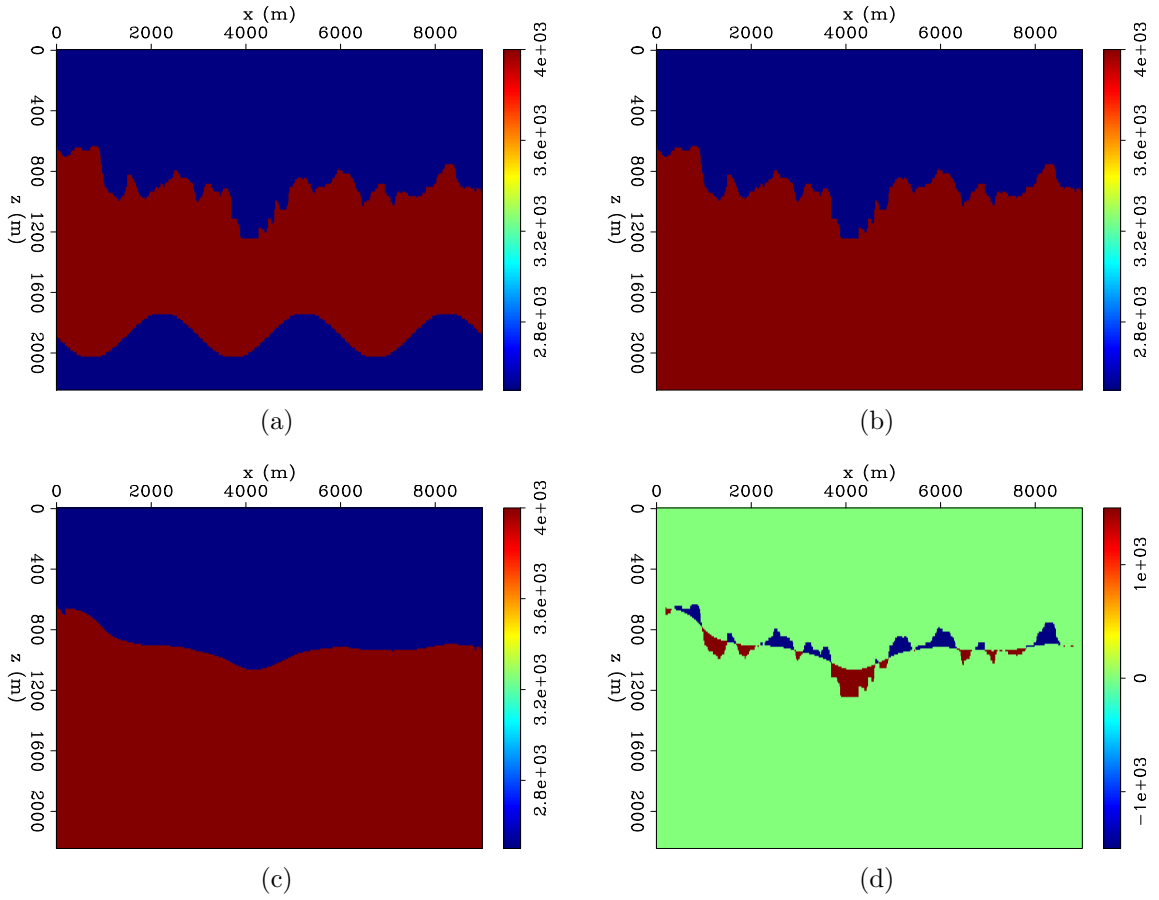

Figure 19: Velocity models modified from the 2004 EAGE velocity benchmark study. (a) True velocity model with a sinusoidal-shape reflector. (b) True background velocity model. (c) Inaccurate background velocity model. (d) Difference between true and inaccurate background velocity models. [**ER**]

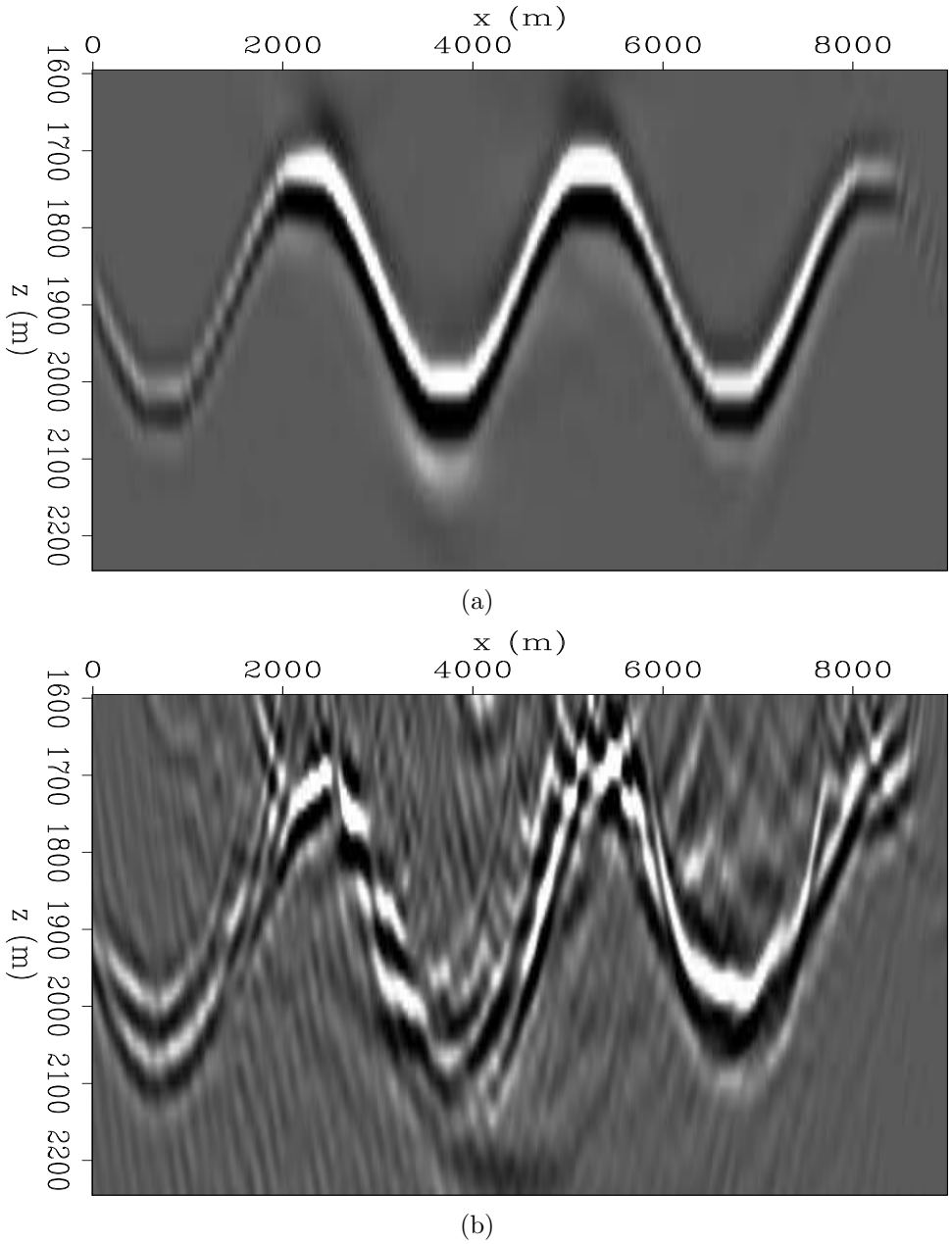

Figure 20: Migrated images. (a) Image computed with the correct background velocity model. (b) Image computed with the inaccurate background velocity model. [**ER**]

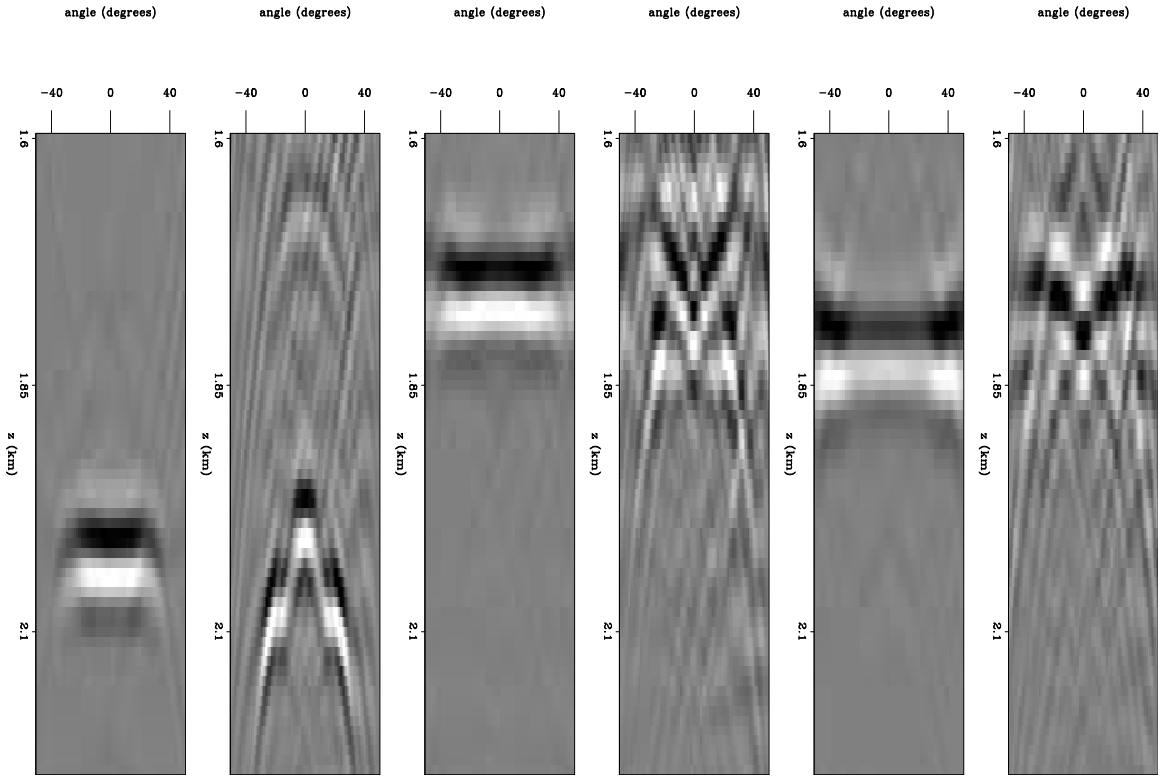

Figure 21: Three pairs of angle domain common image gathers. For each pair, the first image shows the gather computed from the image in Figure 20(a), and the second image shows the gather computed from the image in Figure 20(b). The gathers are computed at $x_1 = 920$ m, $x_2 = 1,196$ m, and $x_3 = 2,760$ m, respectively. [**ER**]

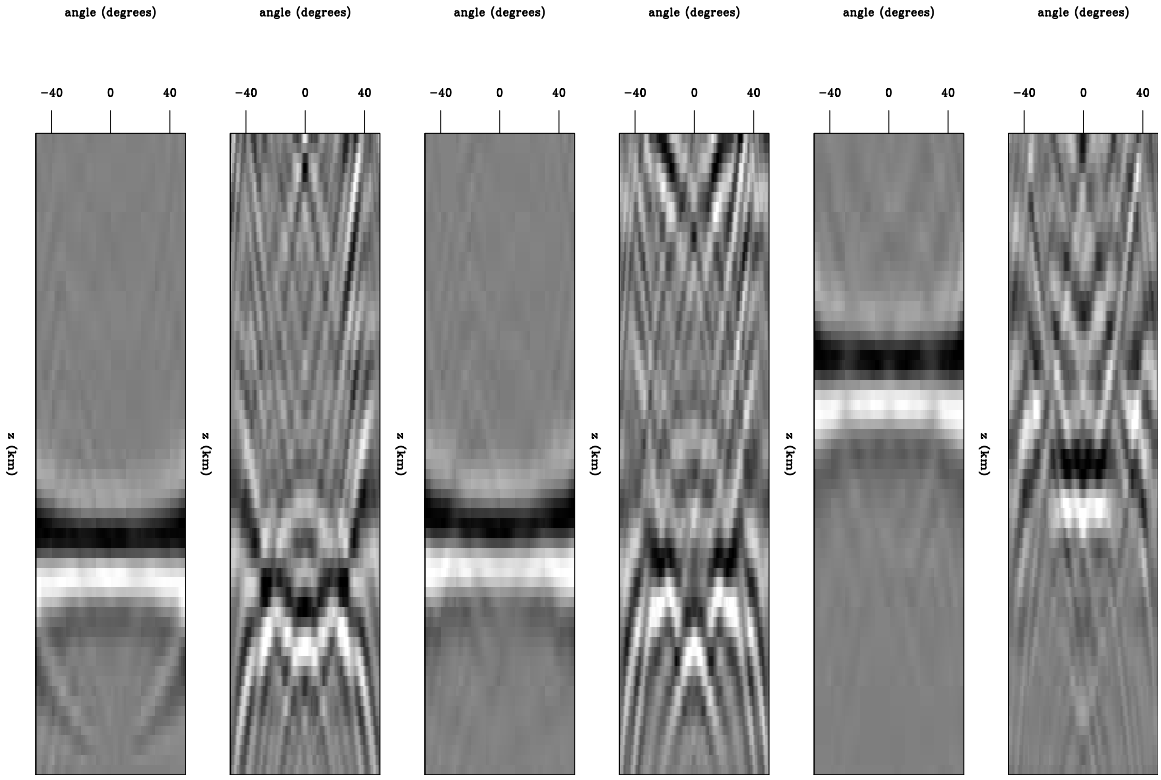

Figure 22: Three pairs of angle domain common image gathers. For each pair, the first image shows the gather computed from the image in Figure 20(a), and the second image shows the gather computed from the image in Figure 20(b). The gathers are computed at $x_4 = 3,730$ m, $x_5 = 4,020$ m, and $x_6 = 4,600$ m, respectively. [**ER**]

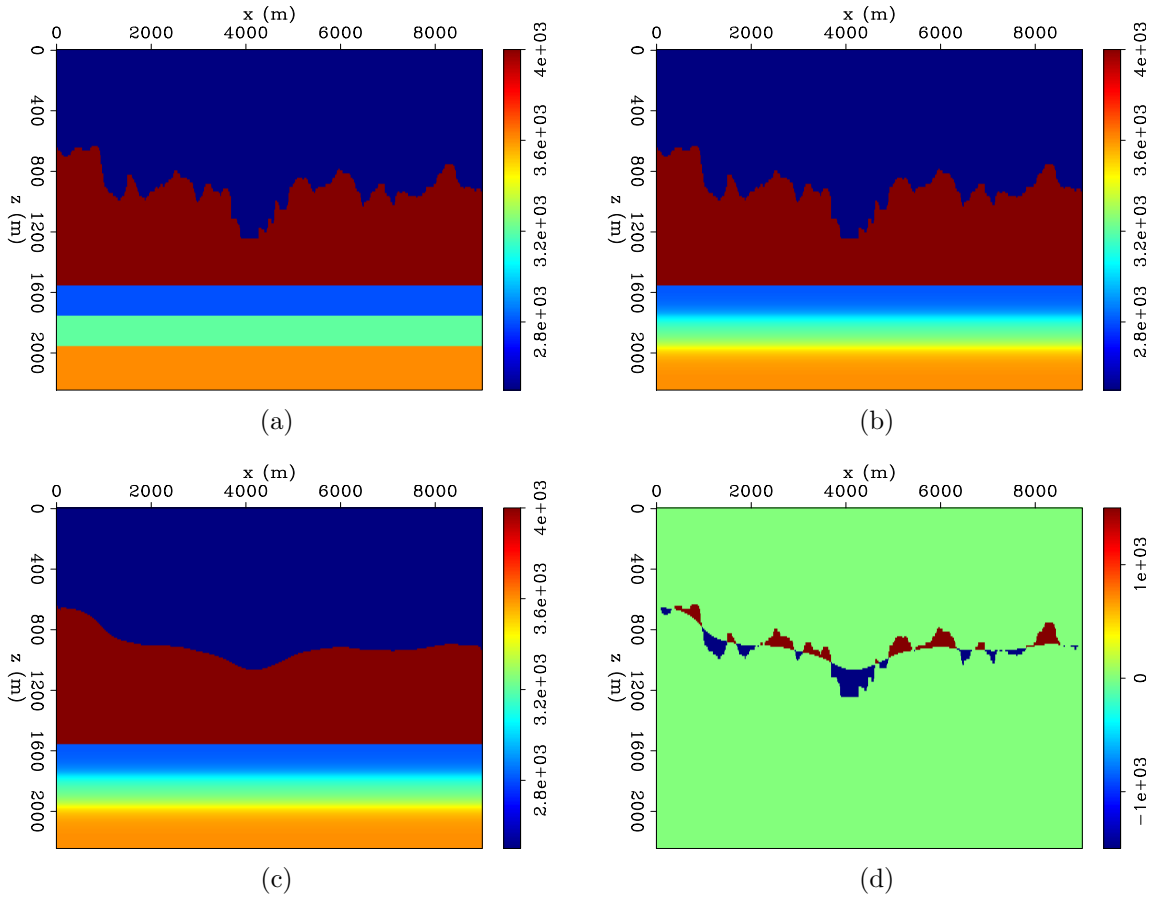

Figure 23: Velocity models modified from the 2004 EAGE velocity benchmark study. (a) True velocity model with two subsalt reflectors. (b) True background velocity model. (c) Inaccurate background velocity model. (d) Difference between true and inaccurate background velocity models. [**ER**]

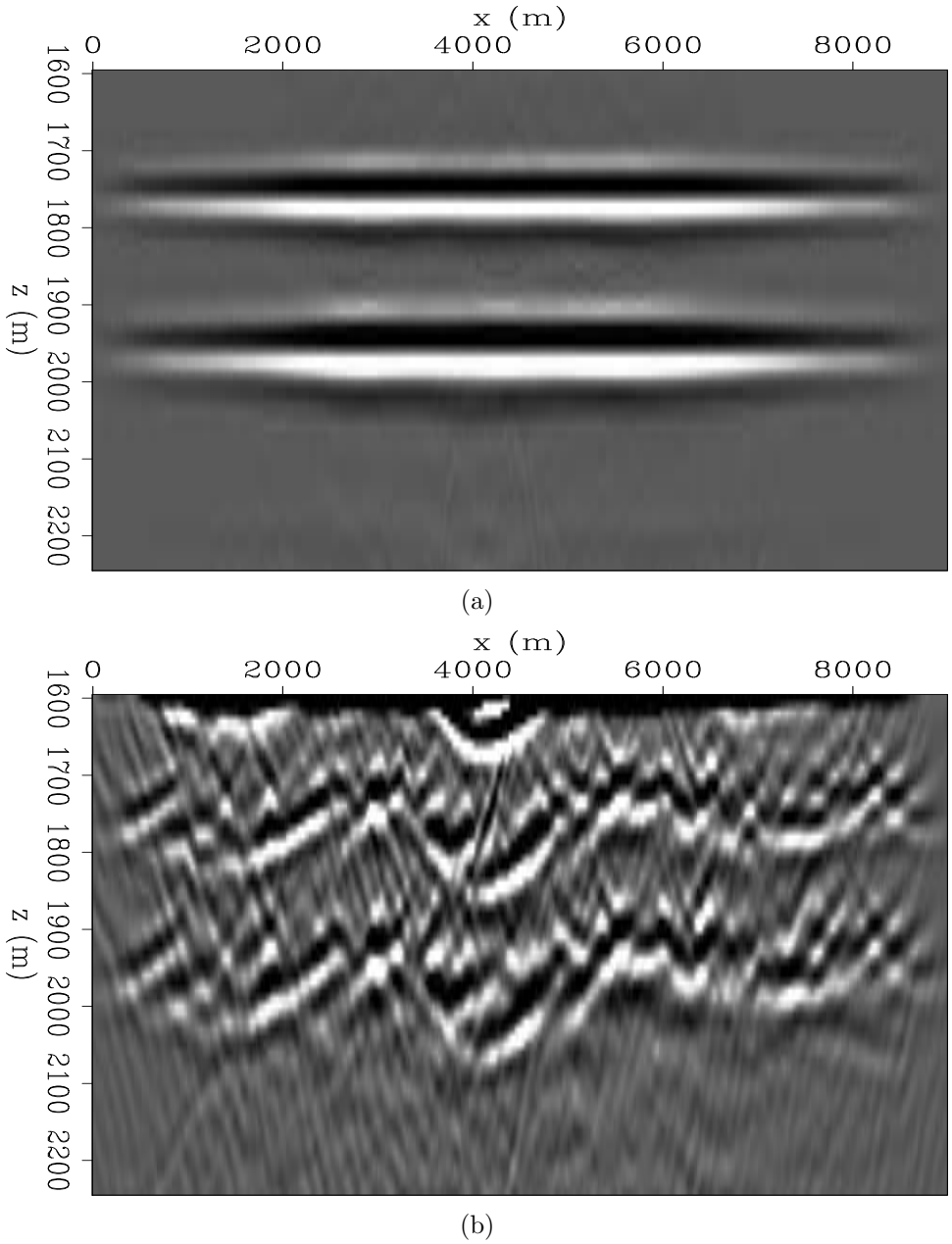

Figure 24: Migrated images of the velocity model in Figure23(a). (a) Image computed with the correct background velocity model. (b) Image computed with the inaccurate background velocity model. [**ER**]

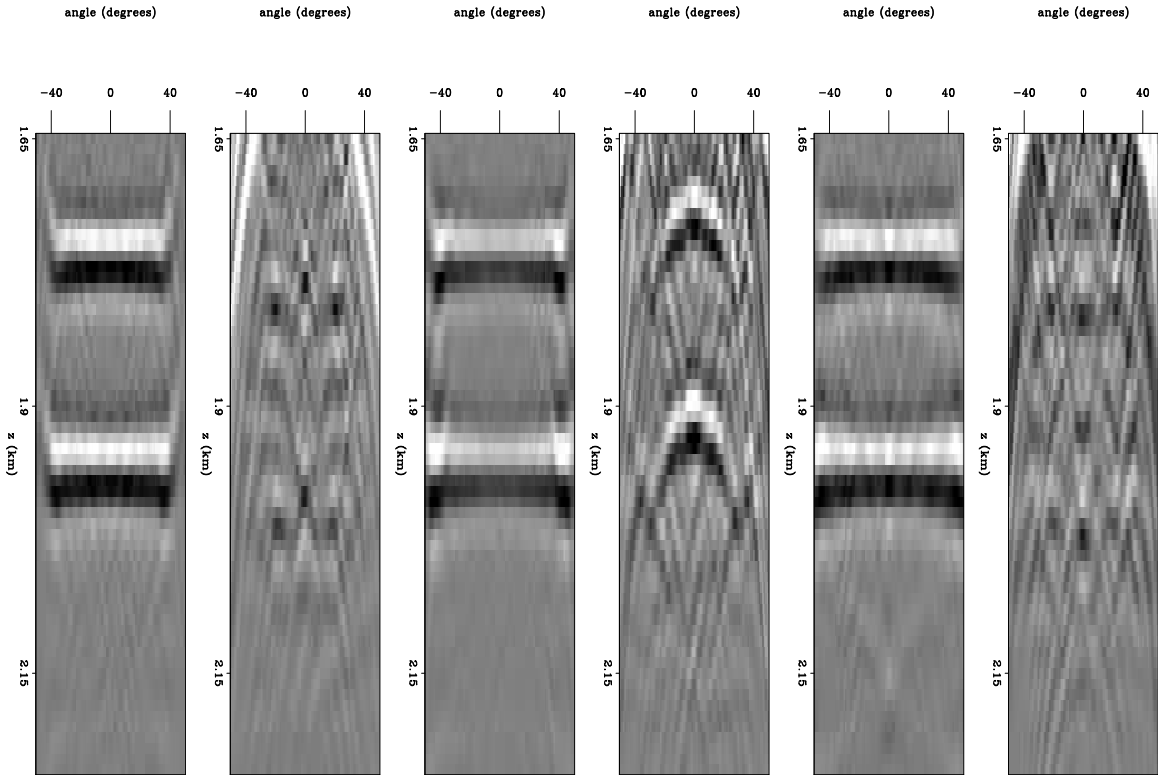

Figure 25: Three pairs of angle domain common image gathers. For each pair, the first image shows the gather computed from the image in Figure 24(a), and the second image shows the gather computed from the image in Figure 24(b). The gathers are computed at $x_1 = 1,730$ m, $x_2 = 2,580$ m, and $x_3 = 3,680$ m, respectively. [**ER**]

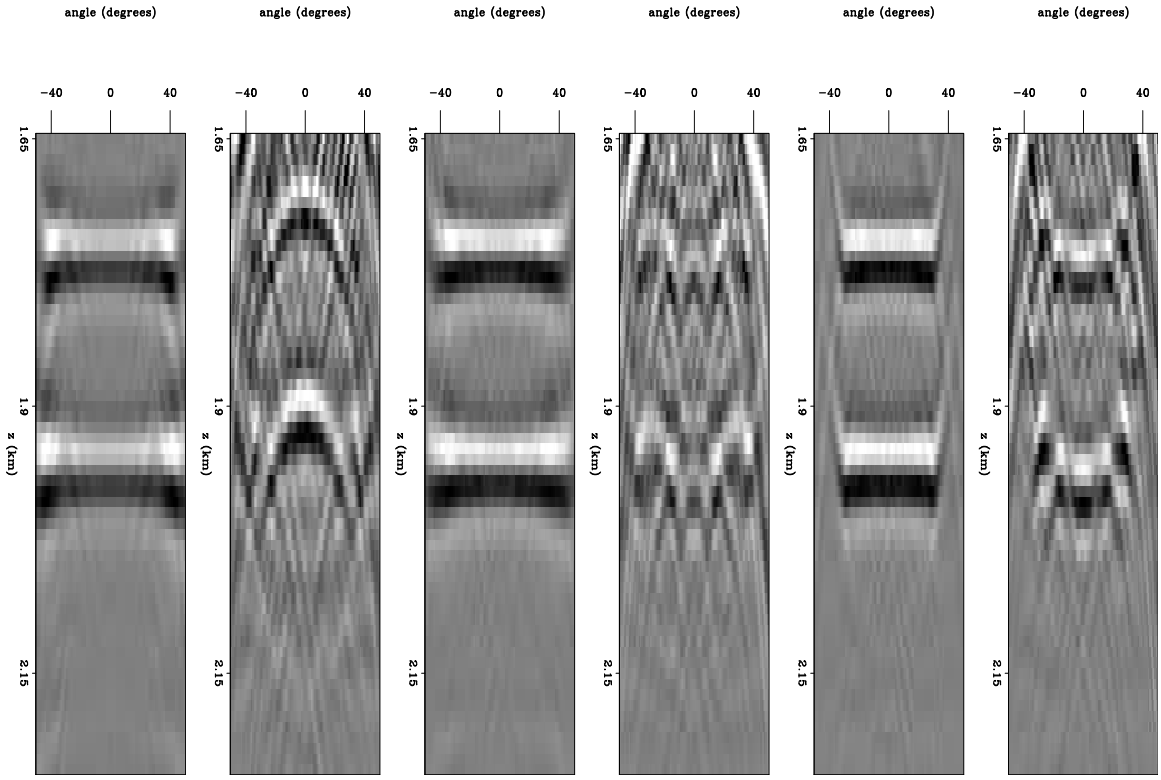

Figure 26: Three pairs of angle domain common image gathers. For each pair, the first image shows the gather computed from the image in Figure 24(a), and the second image shows the gather computed from the image in Figure 24(b). The gathers are computed at $x_4 = 5,980$ m, $x_4 = 6,6670$ m, and $x_5 = 7,550$ m, respectively. [**ER**]

the lack of accuracy in the top-salt boundary does not enable the receiver wavefield to refocus correctly below the salt, which will in turn deteriorate the migrated image. Adding the contributions from all shots will not stack constructively and the resulting image will show very little coherency. This was confirmed by the second set of tests we performed. The images of subsalt layers are extremely sensitive to the accuracy of the salt boundary. Moreover, as mentioned by Etgen et al. (2014b), it is difficult to extract any useful information from extended images because the gathers show no coherency.

CONCLUSIONS AND FUTURE WORK

We discussed why obtaining good-quality seismic images of zones that lie in the vicinity of salt bodies is becoming more and more crucial for the oil and gas industry. We summarized the main difficulties in doing so, and we chose to focus our research on the specific problem related to inaccurate top-salt boundary delineation. We argued that current techniques may still have trouble recovering a rugose sediment-salt interface with enough detail. The synthetic tests we performed confirmed that a slight misinterpretation of the top-salt deteriorates the images of subsalt reflectors to the point where almost no coherent energy is present, even by looking at angle domain common image gathers. This prevents us from successfully applying standard migration velocity analysis techniques. Therefore, there is a need for a new technique that can enable us to directly refocus subsalt images, or at least improve their coherency along an extended axis (e.g., time-lags, subsurface offsets, angle, etc.).

Moving forward, we would like to design an inversion scheme that allows us to bring back coherency along the extended axis of subsalt images, which would then allow us to successfully apply standard migration velocity analysis algorithms (e.g., TFWI). Considering our goal, we believe that an optimization scheme using an image-space objective function (e.g., WEMVA) could be appropriate. However, it can not rely on the presence of interpretable moveout in the extended image domain. A stack power maximization (SPM) scheme looks to offer the most potential. Though this implementation is prone to cycle-skipping, we could potentially circumvent this issue by taking a similar approach as the one done in Biondi and Almomin (2014), and introduce a linearization of the wave-equation based on the extension of the velocity model along the time-lag or subsurface offset axis.

ACKNOWLEDGMENTS

We would like to thank the Stanford Exploration Project affiliate companies for financial support. Guillaume Barnier would like to thank Ali Almomin, Gustavo Alves, Ettore Biondi, Musa Maharramov, Yi Shen, Joe Stefani, and Yang Zhang for their help and advice.

REFERENCES

Albertin, U., L. Zhang, et al., 2014, Migration optimization through local phase alignment of partial migration images: Presented at the 2014 SEG Annual Meeting.

Anselmetti, F. S. and G. P. Eberli, 1993, Controls on sonic velocity in carbonates: Pure and Applied Geophysics, **141**, 287–323.

Biondi, B. and A. Almomin, 2014, Simultaneous inversion of full data bandwidth by tomographic full-waveform inversion: Geophysics, **79**, WA129–WA140.

DNR, 2015, Reservoir traps: Louisiana Department of Natural Resources, http://dnr.louisiana.gov/assets/TAD/education/BGBB/4/traps.html (accessed April 2015).

Dribus, J., M. Jackson, J. Kapoor, and M. Smith, 2008, The prize beneath the salt: Oilfield Review, **15**, 4–17.

Etgen, J. T., I. Ahmed, M. Zhou, et al., 2014a, Seismic adaptive optics: Presented at the 2014 SEG Annual Meeting.

Etgen, J. T., C. Chu, T. Yang, M. Vyas, et al., 2014b, Adaptive image focusing: Presented at the 2014 SEG Annual Meeting.

Farmer, P., D. Miller, A. Pieprzak, J. Rutledge, and R. Woods, 1996, Exploring the subsalt: Oilfield Review, **8**, 50.

Halpert, A. D., 2014, Interpreter-driven automatic image segmentation and model evaluation: PhD thesis, Stanford University.

Hudec, M. R. and M. P. Jackson, 2007, Terra infirma: [u]nderstanding salt tectonics: Earth-Science Reviews, **82**, 1–28.

Jones, I. F. and I. Davison, 2014, Seismic imaging in and around salt bodies: Interpretation, **2**, SL1–SL20.

King, H., 2015, Salt domes: Geoscience News and Information, http://geology.com/stories/13/salt–domes/ (accessed April 2015).

Leveille, J. P., I. F. Jones, Z.-Z. Zhou, B. Wang, and F. Liu, 2011, Subsalt imaging for exploration, production, and development: A review: Geophysics, **76**, WB3–WB20.

Levin, H. L., 2009, The earth through time: John Wiley & Sons.

Ritter, G. et al., 2010, Interpretation driven velocity model building to improve subsalt imaging: Presented at the 2010 SEG Annual Meeting.

Schlumberger, 2015, Subsalt: Schlumberger Oilfield Glossary, http://www.glossary.oilfield.slb.com/en/Terms.aspx?LookIn=term=subsalt (accessed April 2015).